Chapter 1

General Introduction

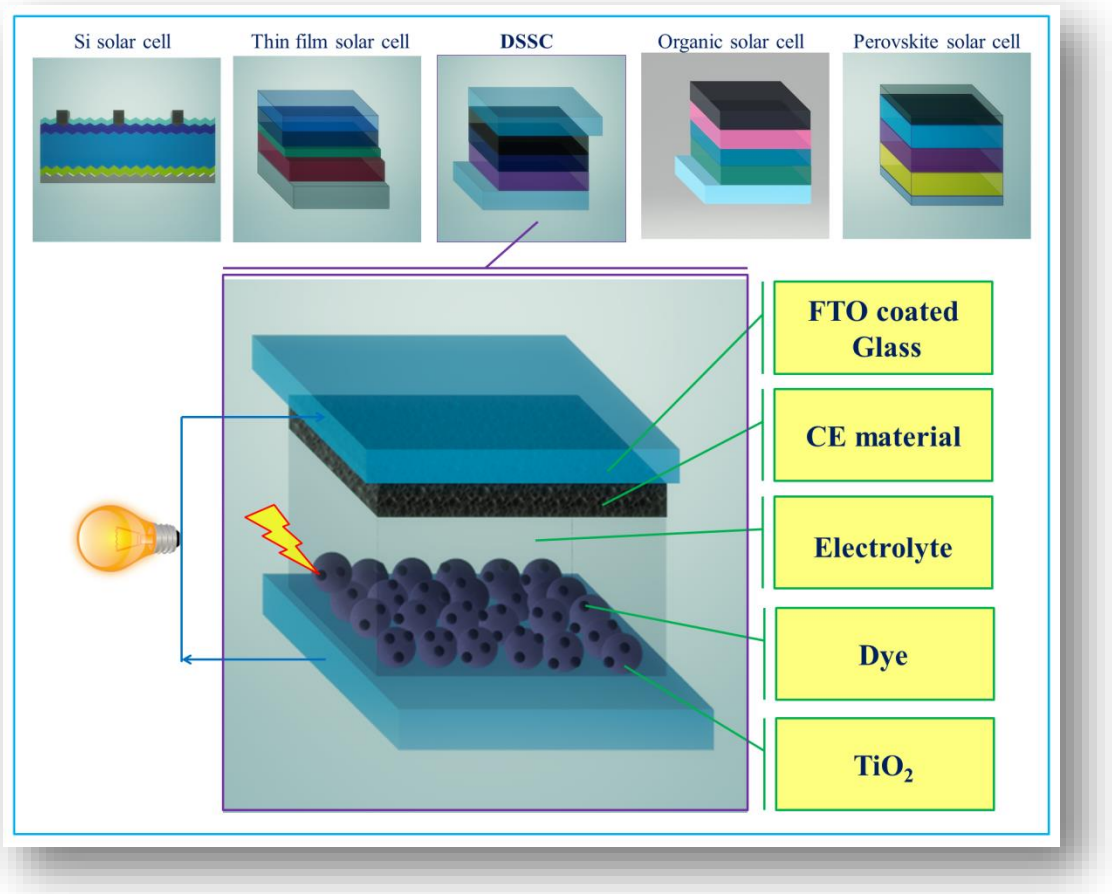

The research background and the motivation for the present investigation are described in this chapter along with brief literature review on the state of the art photovoltaic devices.

1.1 Motivation

In this fast-growing world, energy sources have become the core for smoothly running a normal human life. The global energy consumption will continue to rise in the coming times due to the ever-increasing use of technology and growing industrial energy demands. Presently, the major part of our energy needs is being fulfilled by the non-renewable fossil fuels such as petroleum, coal, natural gas and nuclear power. However, the limited reservoir of fossil fuels is hardly expected to meet the energy demands in the near future. Additionally, they also produce the major contributors to the global warming. The implementation of nuclear power is rather challenging as well because of the safety-related issues of the radioactive materials and the management of the nuclear wastes. These inadequacies of the non-renewable energy sources can be resolved by using renewable energy sources. There are various alternative renewable energy resources such as hydro-power, solar photovoltaics, solar concentrator, solar heater, biofuel, biomass, geothermal, tidal power, wave power and wind power. Amongst them, the energy from photovoltaic (PV) devices is anticipated to play a prominent role in the near future [1,2]. Sun is the largest and the most underutilized electrical power plant we will ever have and it is the prime source of energy for sustenance of life on Earth. The Earth's surface is endowed with about 3×10^{24} Joules of energy annually in the form of sunlight which is statistically almost 10^4 times more than the world's energy consumption. However, barely $1/10^{th}$ of all the energy we consume on Earth comes from the Sun [3,4]. For effective utilization of the abundant solar energy, a practical system is required for photoconversion, storage and distribution of this energy.

1.2 History and development of photovoltaics

1.2.1 Solar radiation

Solar radiation is the incandescent electromagnetic (EM) energy radiated by the Sun due to the nuclear fusion reaction taking place inside its core. Even though very hot on the inside, the temperature gradually decreases towards the surface, from where the emission occurs. The surface temperature is estimated to be about 5800 K. At this temperature, the solar spectrum resembles the spectrum of a black body at 5800 K, and emits EM radiations covering the entire EM spectrum including radio waves, infrared, visible light, ultraviolet (UV) and X-rays. **Figure 1.1** shows the spectra of the solar radiation on the Earth's surface without, and with absorption of some wavelengths by atoms and ions in the atmosphere. The power density of the Sun illumination on an object is defined by *solar irradiance (H_O)*, and its SI unit is W m^{-2}. The value of H_O is indirectly proportional to the distance of the object from the Sun, and can be mathematically represented as below (**Eq. (1.1)**):

$$H_O = (R^2_{Sun} / D'^2)\, H_{Sun} \quad \text{..... (1.1)}$$

where R_{Sun}, D' and H_{Sun} represent the radius of the Sun (in m), the power density at the Sun's surface (in W m^{-2}) and the distance of the object from the Sun (in m). Using this relation, the solar radiation is found to be 1.366 kW m^{-2} on the outside of the Earth's atmosphere.

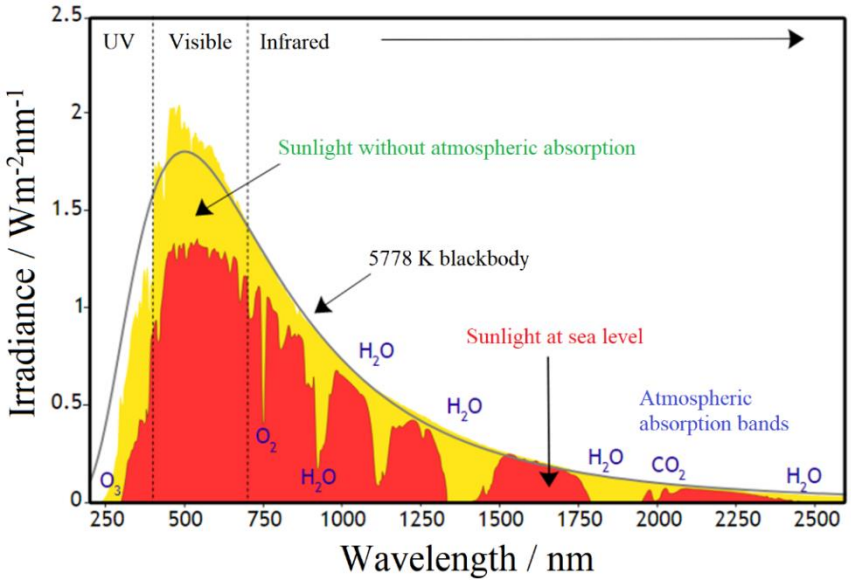

Figure 1.1. Solar radiation spectrum on the Earth's surface [5].

The term *Air Mass (*AM*)* is often used to quantify the reduction of the power of the sunlight due to the absorption in the atmospheric components. AM is defined as the length of the path travelled by the sunlight through the atmosphere relative to the length of the shortest possible pathway of the light (**Figure 1.2**). The Sun right on the top of our head will be the shortest pathway of the light.

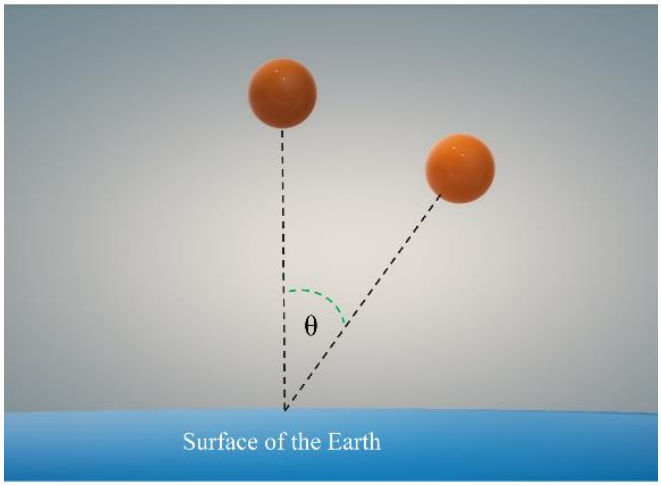

Figure 1.2. Air mass calculated from the zenith point [6].

Mathematically, AM is expressed by **Eq. (1.2)**

$$AM = 1/\cos\theta \quad \textbf{(1.2)}$$

Here, the *elevation angle (θ)* represents the angle of the light ray from the vertical position. The value of AM is 1 when θ = 0; that is when the light is traveling through the shortest possible path with maximum power of light [6]. AM 1.5G is used as a standard spectral distribution at the surface of the Earth (G stands for global, and includes both the diffuse and direct radiation), and AM 1.5D is used for direct radiation (D) only. For AM 1.5G, θ = 48.2° and the difference of the path length of the light is 1.5 times higher than that of AM 1G. The thickness of the atmosphere decreases the value of H_O to 970 W m^{-2} for AM 1.5G. However, for convenience, this standard global spectrum is normalized to 1000 W m^{-2}, and accepted as standard 1 Sun illumination at the Earth's surface. Consequently, 1000 W m^{-2} is used in solar simulators to record the performances of solar cells in laboratories.

1.2.2 Development of photovoltaics

The direct conversion of sunlight (photo-) to electricity (-voltaic) is termed as *photovoltaics*, and the devices exhibiting this effect are known as *photovoltaic* (PV) *devices*. The interest in the field of "*photovoltaics*" is not recent. In 1839, Alexandre-Edmond Becquerel discovered the PV effect, and invented the first PV cell at the age of 19. The photo-electrochemical cell was prepared by immersing platinum electrodes in an electrolyte comprising silver chloride in an acidic medium. The same cell generated voltage and electrical current under irradiation of light. Because of his invaluable contributions, the PV effect is also known as the *Becquerel effect* [7]. The growth of PV technology actually jump-started with the invention of the first practical silicon based PV cell by Bell Laboratories in 1954. The cell exhibited 6% photoconversion efficiency [8]. Since then, a steady growth of the PV industries has afforded subsidized electrical energy in urban areas as an on grid and off grid technology.

The global expansion of the PV industries over the last two decades can be understood from the snapshot of global PV: 2017 released by the International Energy Agency (IEA) [9]. According to this report, the PV market has created new records by nearly attaining the 100 GW threshold. The continuous growth of PV market has been highly influenced by the input from China. With the installation of 53 GW PV modules, it contributed to 54% of the total installed capacity in the year 2017 (**Figure 1.3**). The United States of America with solar module installation of 10.6 GW and India with 9.1 GW held the second and the third positions respectively, thereby establishing Asia as the leader in the PV market.

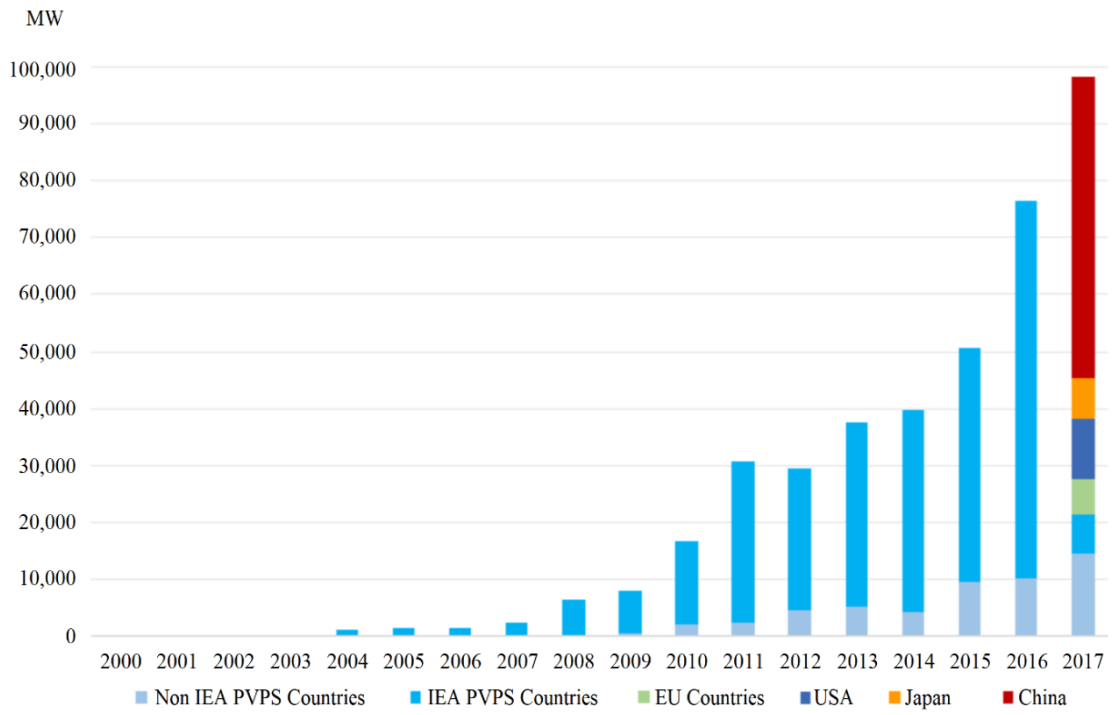

Figure 1.3. Growth of world's photovoltaic market [9].

1.2.3 Theoretical limit of the efficiency of solar cells (Shockley-Queisser limit)

The performance of a solar cell is evaluated by its efficiency of conversion of the incident light energy into electrical energy. The efficiency of a solar cell depends highly on the properties of the semiconductor materials. The maximum theoretical efficiency of single p-n junction based PV cell can be determined by using the *Shockley-Queisser limit* (SQL), also known as the *detailed balance limit*. This important concept of a theoretical efficiency limit was first introduced by William Shockley and Hans-Joachim Queisser in the year 1961 [10]. SQL is related to the band gap of the semiconductor material used to fabricate the PV cell. **Figure 1.4** shows the variation of the limit with changing band gaps. Ideally, a single p-n junction solar cell can have the maximum theoretical limit of 33.16% for AM 1.5G illumination, and entails a semiconductor with a band gap of 1.34 eV [11]. The most common semiconductor material for PV cell, silicon with a band gap of 1.1 eV shows a theoretical efficiency limit of approximately 32%. However, the current practical monocrystalline silicon PV cells exhibit only about 24% of efficiency.

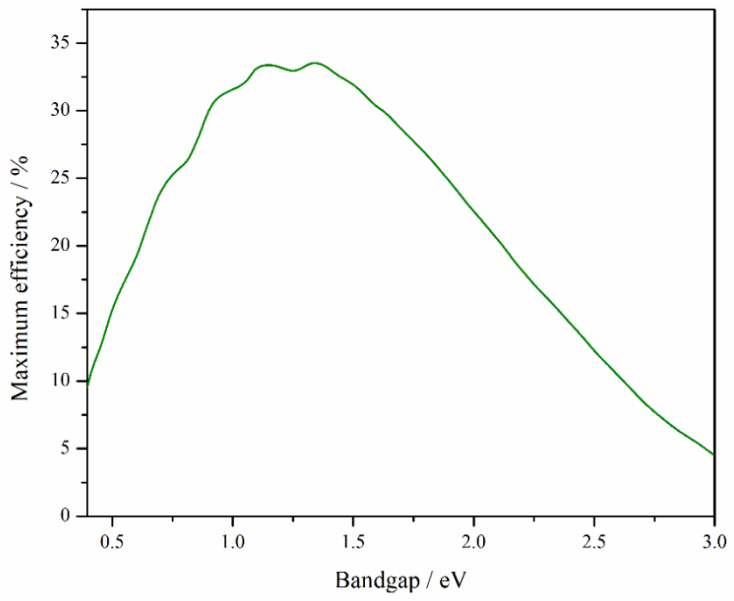

Figure 1.4. Variation of efficiency with bandgap of different semiconductor materials [11].

1.3 Classification of solar cells

At present, the field of photovoltaics has extended to include many new types of solar cells, other than the traditional silicon based cells. They are classified into three generations on the basis of the device structure and the materials used to fabricate these cells.

1. **First generation**: PV cells based on crystalline silicon. Both monocrystalline and polycrystalline silicon are used as a semiconducting material to fabricate the cells.
2. **Second generation**: PVs cells based on thin film technology. The foremost semiconductor materials used in this type of cells are amorphous silicon, copper indium gallium selenide (CIGS) and cadmium telluride (CdTe) [12,13].
3. **Third generation**: Emerging PV technologies like [14–20]
   (a) organic solar cells,
   (b) dye sensitized solar cells,
   (c) quantum dot solar cells, and
   (d) perovskite solar cells.

The PV solar cells can also be categorized into two sections depending on their working principles.

1. **Conventional p-n junction solar cells**. Sunlight is absorbed by an inorganic semiconductor to excite an electron across the semiconductor bandgap. This category includes the first and the second generation solar cells.
2. **Excitonic solar cells**. Sunlight is absorbed by a polymer (organic solar cell), a dye molecule (dye sensitized solar cell) or a quantum dot (quantum dot solar cell) to generate

an exciton. The exciton then dissociates across a hetero-interface and generates charge carriers.

1.3.1 Conventional p-n junction solar cells

To generate electrical energy from photon energy in any type of solar cell, the occurrence of three main processes is essential:

a) absorption of photon energy,
b) separation of the photogenerated electron-hole pairs, and
c) collection and extraction of free charge carriers at the two electrodes.

Figure 1.5 shows the band diagram of a conventional p-n junction solar cell under irradiation of light. The penetration of a photon is directly proportional to its wavelength. Photons with sufficient energy can excite the electrons from the valance band to the conduction band, leaving behind positively charged holes in the valance band. If the electron-hole pairs are generated in the depletion region, the presence of the electric field in this region causes the electrons to move toward the n-side and the holes toward the p-side, resulting in charge separation. Electron-hole pairs are also created outside the depletion region (in the p- and the n-regions). These carriers generated in the p- and the n-regions diffuse to the space charge region and contribute to the output current. Finally, the separated charges carriers are collected at the two electrodes [21,22].

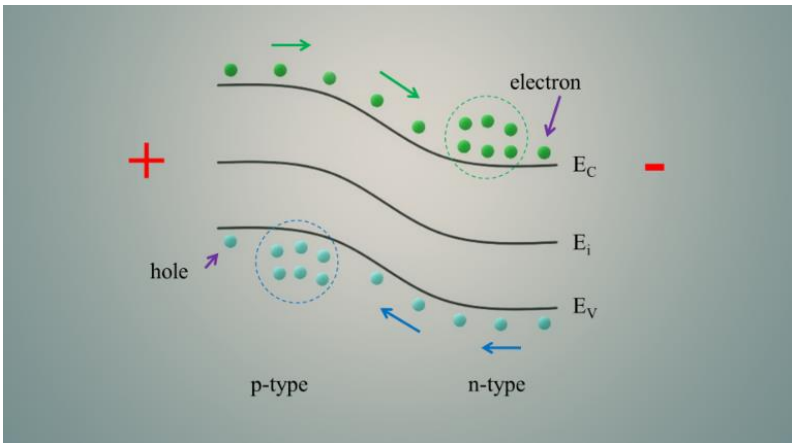

Figure 1.5. Band diagram of a p-n junction solar cell under irradiation of light [6].

1.3.1.1 First generation solar cells

Most of the solar modules on our rooftops belong to the first generation silicon wafer based PV technology. This first generation practical silicon based solar cell was first introduced by an American physicist working for the Bell Laboratories, Russell Ohl in 1954 which showed an efficiency of 6%. These cells occupy a major share in the PV market due to their high

efficiency and durability. Only pure form of silicon is used in solar cells. Although silicon is the second most abundant element in the Earth's crust, its availability in the pure form is very rare. Usually, silicon is found in the form of silica (silicone dioxide) or silicates. The purification process of silica to pure silicon consumes huge energy which raises the cost of the cell [23]. In the market, two types of crystalline silicon based solar cells are available: monocrystalline silicon and poly-crystalline silicon. To produce highly pure monocrystalline silicon wafers, Czochralski technique (also known as ingot drawing process) is used [24,25]. The polycrystalline silicon wafers are made using various techniques like ingot casting and ribbon drawing [26–28].

The first generation solar cell works on the principle of a p-n junction. The top side in silicon solar cell is considered the n-region. Light is incident on this side, hence to ensure better light penetration, this region is usually kept thin and highly doped. The p-region, on the other hand, is thick in size and poorly doped. The basic cross-section of a monocrystalline silicon solar cell is shown in the **Figure 1.6**. Monocrystalline silicon based solar cells exhibits higher efficiencies than poly-crystalline silicon based solar cells. The most efficient monocrystalline silicon solar cell shows about 25% of efficiency [29].

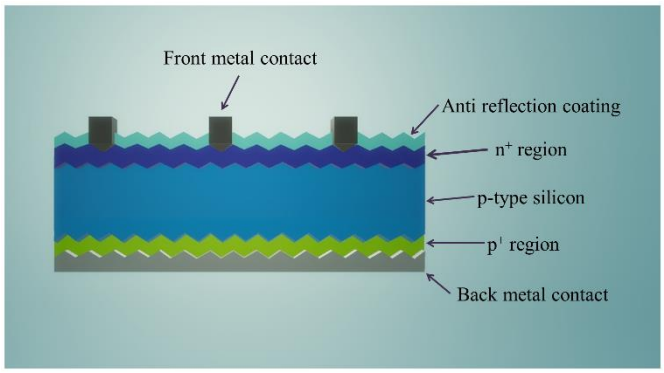

Figure 1.6. Cross-section of a basic monocrystalline silicon solar cell [29].

1.3.1.2 Second generation solar cells

The thin film solar cells are considered as the second generation PV cells. The high cost of using thick wafer of pure crystalline silicon the first generation cells has led to the development of thin film technology, where very thin active semiconductor layers are deposited on a supporting substrate. The requirement of the quantity of the costly materials is reduced and at the same time, cells can be made flexible. Various physical (thermal evaporation, sputtering process etc.) and chemical (chemical vapour deposition) deposition techniques are available to make the thin film layers on the substrates. These films can be deposited at a comparatively lower temperature than the traditional silicon wafer based cells. Moreover, the cell and the module making process is the same, while in case of silicon wafer based technology, the modules are made by integrating many cells in a series. The active material properties, such as band gap,

conductivity, diffusion length and electron lifetime can be tuned to optimize the cell performances. For use as substrates, transparent conducting oxide (TCO) glass, flexible plastic and even metal are employed so as to minimize the current loss in thin film cells due to the substrates' high sheet resistances [30–32].

Based on their structures, there are primarily four types of thin film PV devices:

a. p-n junction with same materials (homo-junction cell),
b. p-n junction with different materials (hetero-junction cell),
c. p-i-n junction (amorphous silicon based solar cell, here i represents intrinsic), and
d. multi-junction thin film cells [33–36].

The p-n junction thin film solar cells follow the same charge separation mechanism as conventional silicon cells. However, amorphous silicon based cells follow p-i-n junction principle. This is due to the fact that their charge separation depends on the *drift* mechanism rather than the *diffusion* mechanism because of the low lifetime of the carriers. This can be described by using the band diagram of the p-i-n junction (**Figure 1.7**).

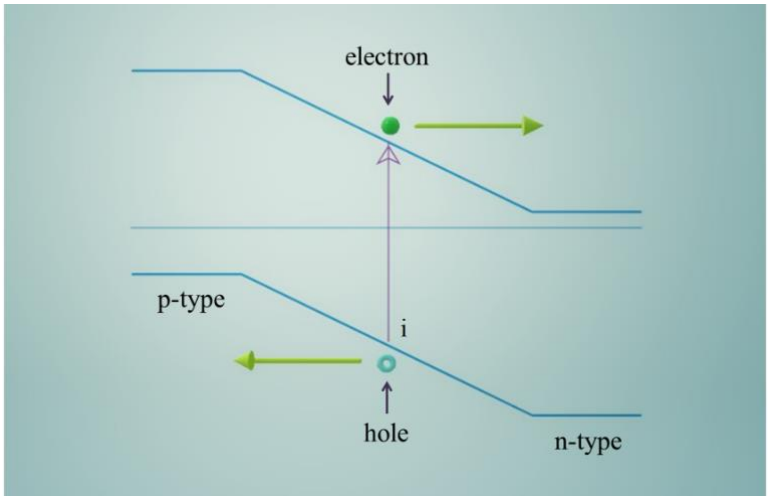

Figure 1.7. Band energy diagram of p-i-n junction under irradiation of light.

When electron-hole pairs are formed at the intrinsic region under irradiation, the electrons drift to the n-region and the holes drift to the p-region because of the electric field generated at the intrinsic amorphous silicon region. This electric field then helps to separate the photogenerated election-hole pairs with low lifetime [37].

Cadmium sulfide (CdS), cadmium telluride (CdTe), copper indium gallium selenide (CIGS) or copper indium gallium diselenide ($Cu(In,Ga)Se_2$) and amorphous silicon are frequently used in thin film technology [38–40]. Maximum laboratory efficiency of 20.3% has been achieved using CIGS thin film solar cells [41]. **Figure 1.8** shows the typical structure of thin film solar cells.

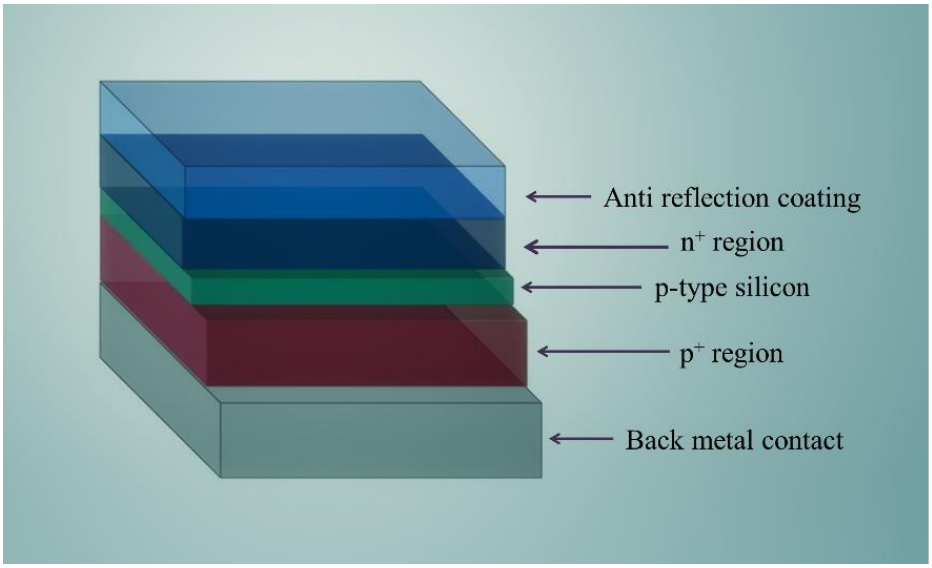

Figure 1.8. A typical structure of a thin film solar cell.

1.3.2 Excitonic solar cells

Excitonic solar cells are an interesting class of PV cells which includes the emerging classes of third generation solar cells [42–45]. An exciton is defined as a tightly bound electron-hole pair [42]. The main difference between the conventional p-n junction solar cells and the excitonic solar cells lies in the mechanism involved in the generation and separation of charge carriers. The working of an excitonic cell is primarily controlled by interfacial process whereas bulk processes govern the working in conventional p-n junction solar cells [46]. In excitonic cells, charge carriers are formed at the hetero-interface from simultaneous separation of the photo-generated excitons on irradiation, while in the conventional p-n junction cells, the generation of carriers occurs in the bulk [46,47].

The performance of an excitonic cell is independent of the bulk properties like crystallinity and chemical purity. Hence, they can be fabricated using inexpensive less pure materials which lower the cost of the cell.

On irradiation of light of specific energy on an organic material, an exciton (also called *Frenkel exciton* or *mobile excited state*) is generated instead of a free electron-hole pair. The production of excitons is primarily due to two reasons [46,47].

(a) There is significant spreading of the influence of the attractive Coulomb potential well around the photogenerated electron–hole pair due to the low dielectric constant of the organic phase.

(b) A spatially restricted wave function of an electron is generated as a result of the formation of a narrow bandwidth due to the weak non covalent interactions between the organic molecules. This restricted electron's wave function confines the electron in its

conjugated hole's potential well (and vice versa) resulting in an electron-hole pair with a strong attraction.

The energy associated with the initially formed exciton is defined as the *optical bandgap* (E_{opt}) (**Figure 1.9**). Excitons are associated with a large *exciton binding energy*. The *electrical bandgap* (E_{bg}; threshold energy for generating a free electron and hole from an exciton) for organic semiconductors is the combination of optical bandgap and exciton binding energy as shown in **Figure 1.9.** The effective *bandgap of the hetero-junction* is denoted as E_{bghj}. The excitons do not have sufficient energy to separate in the bulk, but at the hetero-interface (interface between p-type and n-type semiconductor), the excitons dissociate to free electrons and free holes *via* an exothermal pathway. This results in accumulation of electrons in the n-type side and holes in the p-type side of the hetero-interface**,** which contribute to its efficiency. The dissociation of excitons occurs only when the band offset is equal to or greater than its binding energy.

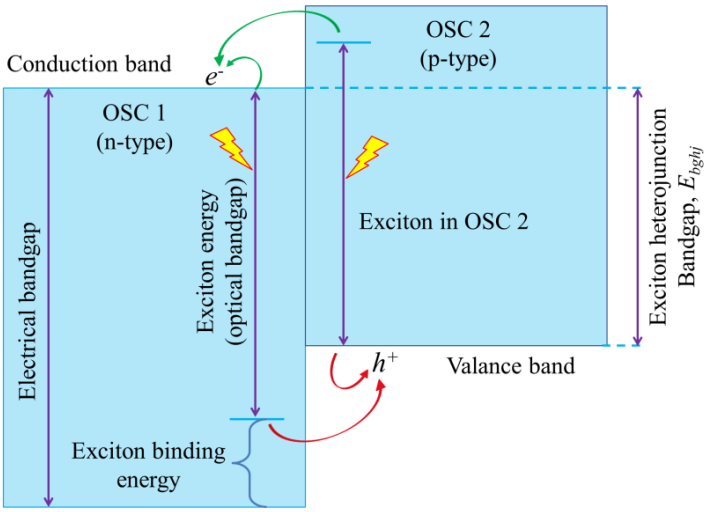

Figure 1.9. Energy level diagram of an excitonic solar cell under illumination of light [48].

1.3.2.1 Organic solar cells

Organic solar cells, also known as *polymer solar cells*, are fabricated by using conducting organic polymer materials. The high optical absorption coefficient of the organic materials, tunable band gap (by modifying the length and functional groups), light-weight nature of the cells are the major advantages of this type of PV cells [17,49–51]. Some of the reported polymer materials (donor/acceptor) include poly(3,4-ethylenedioxythiophene) polystyrene sulfonate (PEDOT:PSS), fluorinated benzothiadiazole and fluorinated fused subphthalocyanine dimer [49,52,53]. The highest efficiency shown by any organic PV device is around 11% [49].

Electron donor and acceptor organic materials are used in the organic solar cells instead of a p-n junction with inorganic semiconductor materials. The highest occupied molecular orbital (HOMO) and the lowest unoccupied molecular orbital (LUMO) of an organic conducting polymer acts as the valance band and the conduction band respectively. The energy difference between the HOMO and the LUMO is considered as the bandgap of that material. There are different kinds of organic solar cells based on their junction type like

- single layer,
- bilayer, and
- bulk hetero-junction, etc.

A high work function electrode (e.g., indium tin oxide, ITO) is used along with a low work function electrode (e.g., aluminum, magnesium, calcium, etc.) to fabricate the device. The difference in the work function creates an electric filed which helps to separate the electron-hole pairs from the photogenerated excitons. In a bilayer organic solar cell, the active layer is formed by having two layers of materials with different ionization energies and electron affinities. This creates an additional electric filed which improves the charge separation of the electron-hole pairs. The electrons then fall to the conduction band of the acceptor material from the absorber or the donor. A typical device structure of an organic solar cell is shown in **Figure 1.10**.

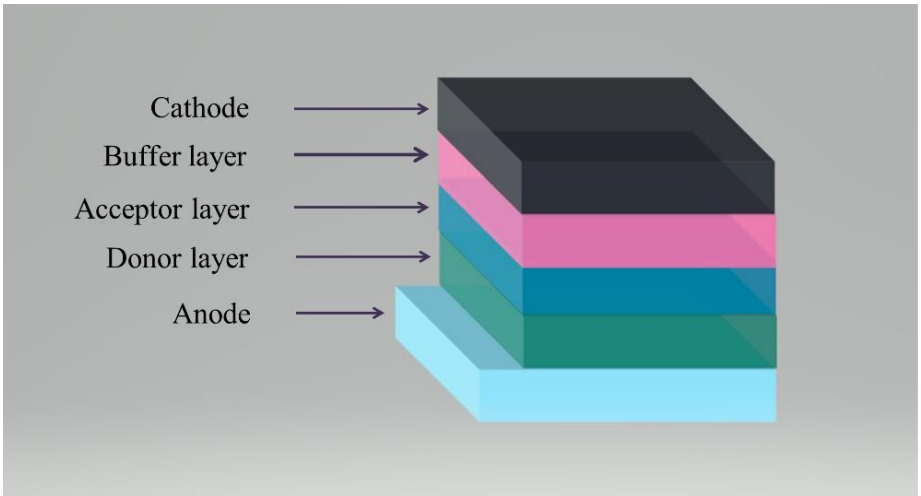

Figure 1.10. A typical device structure of an organic solar cell.

1.3.2.2 Dye sensitized solar cells

During the photosynthesis process, plants produce sugar and oxygen from water and carbon dioxide molecules in the presence of sunlight. This process is made feasible by a green pigment called *chlorophyll*, and is responsible for conversion of the photon energy of sunlight into chemical energy in in the form of glucose. Inspired by the important role played by chlorophyll in natural photosynthesis, Michael Grätzel and Brian O'Regan introduced a new type

of PV cell in which dye molecules play the major role in conversion of solar energy into electrical energy. In 1991, they published their pioneering work on dye sensitized solar cells (DSSCs) which exhibited efficiencies of 7.1-7.9% [54]. The dye molecules in the cell act as a sensitizer, hence the name. The concept of generation of electricity from organic dye molecules under irradiation of light has existed since 1960, when dye molecules were used to produce electricity at oxide electrode under irradiation of light in an electrochemical cell [55]. The principle of generation of electricity in such device was first demonstrated in the University of California in 1972 [56,57]. However, Grätzel and Brian O'Regan were the first to successfully fabricate a practical device with significant efficiency. The cell is also called the *Grätzel cell* to recognize his huge contribution in this field. The DSSC is a third generation PV cell, and a highly researched topic in solar energy because of its easy fabrication technique and low cost.

1.3.2.3 Quantum dot solar cells

In quantum dot solar cells, quantum dots play the key role of converting light energy to electrical energy. The modifiable band gap of quantum dots provides tunable absorption range of light. Because of this property, multi-junction quantum dot PV devices can be fabricated. Quantum dots can be used in different ways.

- As photoanode (containing only quantum dot).
- As photoanode prepared with semiconductor materials (titanium dioxide, TiO_2) adsorbed with quantum dot (the quantum dot acts as a sensitizer). In quantum dot sensitized solar cell, multiple generation of excitons leads improvement of efficiency.
- Cells with blend of quantum dot and electron or hole transporting materials.

The easy synthesis procedures of the colloidal quantum dots, and easy cell fabrication techniques like spray printing and roll printing lower the cost of these cells. 3-D arrays of quantum dots (colloidal and epitaxial) can also be used to fabricate efficient PV cells [58]. The highest reported efficiency obtained with quantum dots has reached 10.6% [59].

1.3.2.4 Perovskite solar cells

The perovskite solar cells are becoming an attractive research area because of their significant efficiencies comparable to that of the conventional silicon based PV cells [20]. These cells contain a perovskite structured material which plays the role of the light absorber and generator of the charge carriers. Organo-lead halide perovskites with outstanding absorption coefficients are very popular as active materials. The most commonly used perovskite absorber is methylammonium lead trihalide ($CH_3NH_3PbX_3$; here X represents halogen atoms like chlorine, bromine or iodine). The bandgap of the material changes from 1.5 to 2.3 eV depending upon the halogen present in the crystal [60–63]. The basic crystal structure of the perovskite

($CH_3NH_3PbI_3$) is ABX_3 type and is shown in **Figure 1.11.** The methylammonium cation ($CH_3NH_3^+$) occupies the central *A* position with an extended frame of corner-sharing PbI_6 octahedra. It is surrounded by 12 nearest-neighbor iodide ions.

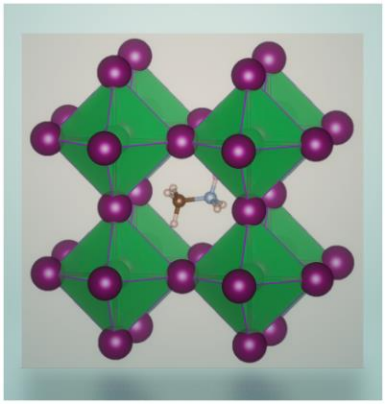

Figure 1.11. Crystal structure of the perovskite ($CH_3NH_3PbI_3$) [64].

The first perovskite solar cell was based on the DSSC architecture. It was introduced by Tsutomu Miyasaka group in 2009 [65]. But that cell showed an efficiency of only 3.8%. The perovskite material was dissolved in the electrolyte, so the durability of the cell was also very poor. Henry Snaith and Mike Lee were able to improve the durability of the cell (with an efficiency of 10%) by replacing the electrolyte with a hole transporting material. They also found that the perovskite itself could transport electrons [66]. In 2016, Korea Research Institute of Chemical Technology (KRICT) and Ulsan National Institute of Science and Technology (UNIST) researchers in South Korea fabricated a single junction perovskite solar cell with the highest certified efficiency of 22.1% [67]. The architecture of different types of perovskite solar cell is in shown in **Figure 1.12**.

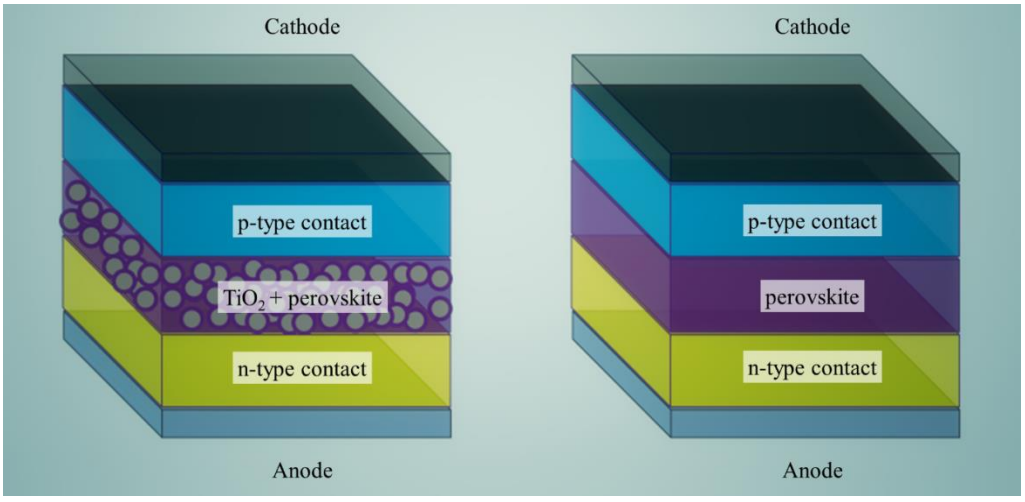

Figure 1.12. Architecture of two different types of perovskite solar cells.

1.3.3 Comparison of efficiencies of different types of solar cells

The efficiencies of different types of solar cells fabricated in various research laboratories over the last 40 years are represented in **Figure 1.13**. The four junction cells with concentrator facilities exhibit the highest efficiency of 46%. However in spite of exhibiting comparatively lower efficiencies, crystalline silicon based solar cells are more popular in the PV market due to their lower cost as compared to the expensive multi-junction cells. Thin film devices and the other emerging third generation PV cells display efficiencies in the range of 14 to 23.3%.

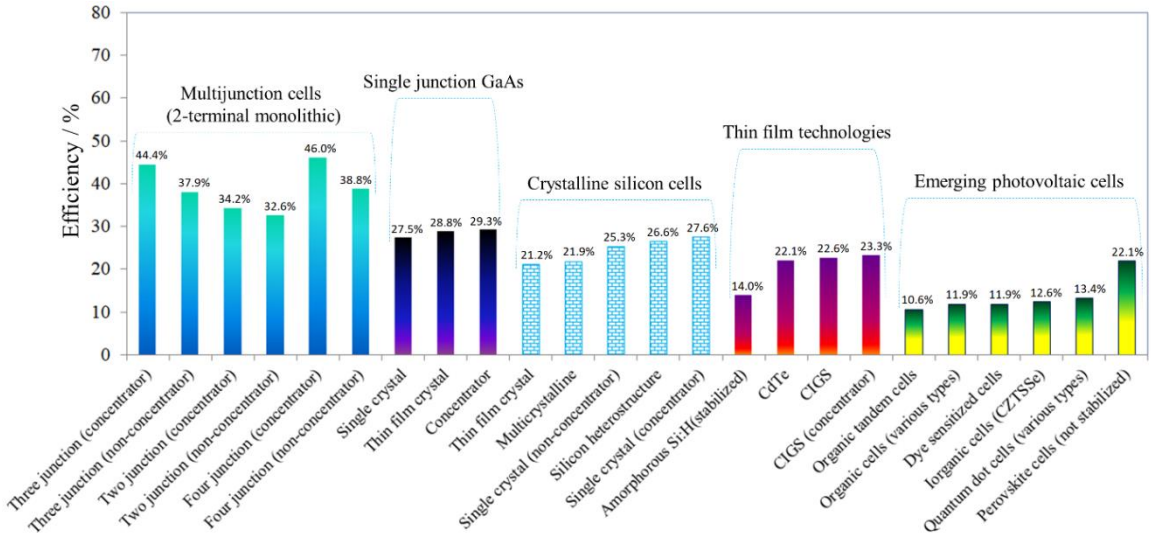

Figure 1.13. Efficiencies of different kinds of PV cells [67].

1.4 Device structure and working principle of DSSCs

The performance of any solar cell depends on three main factors:

1. The absorption of the incident sunlight by the cell. To become a good quality solar cell, the materials used must have good absorption coefficient.
2. Under the irradiation of light, the cell must generate significant number of charge carriers, and the separation of the generated charge carriers should occur properly in the cell.
3. Proper collection of the charges must occur at the electrodes to get considerable electric current output.

The device structure of a DSSC is constructed by considering these three factors. A typical structure of a DSSC composed of three main components:

(a) **a photoanode** (a wide band gap semiconductor with adsorbed dye molecules),

(b) **a counter electrode,** and

(c) **an electrolyte with a redox couple**.

Usually a DSSC is fabricated by placing the electrolyte in between the two electrodes using a spacer, and sealed to prevent the leakage of the electrolyte. The device structure is shown

in **Figure 1.14.** The dye molecules in the photoanode absorb the sunlight and generate photoexcited electrons at the conduction band, and simultaneously act as collector of charge carries. The electrolyte provides an appropriate medium for transportation of the inner charge carriers (redox ions) during the cell's operation. The stability of the cell and the observed current under irradiation is also dependent on the nature of the composition of the electrolyte. The counter electrode of a DSSC reduces the oxidized charge carriers (oxidized ions of the redox couple) to complete the outer circuit. All the three parts are equally important, and the efficiency of a DSSC is either directly or indirectly depends on the quality of these three parts.

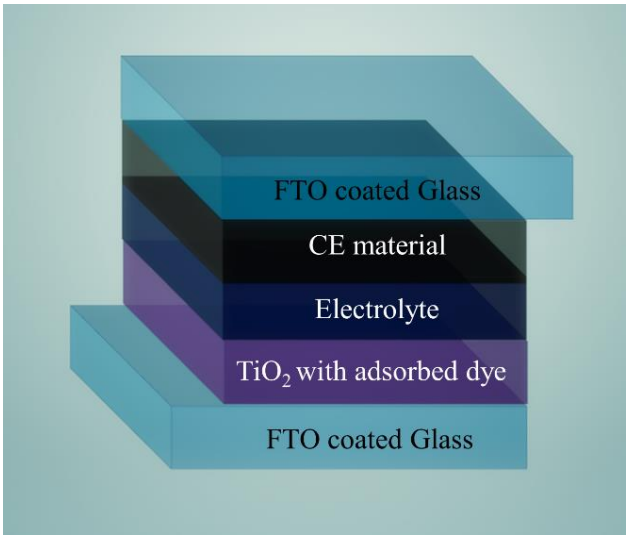

Figure 1.14. Device structure of a typical DSSC.

1.4.1 Device components of DSSCs

1.4.1.1 Photoanode

A thin layer (~10 μm) of a wide bandgap semiconductor material adsorbed with dye molecules on a TCO glass substrate usually serves as the photoanode in DSSCs [68]. If the film thickness exceeds 10 μm, the diffusion length of electrons decreases thereby increasing the electron recombination process.

1.4.1.1.1 Semiconductor

The semiconductor material serves two purposes in a DSSC:

1. It acts as a support for uniform adsorption of the sensitizer dye molecules. To ensure high loading, it is necessary to employ materials with high surface areas.
2. It also aids in the transportation of photoexcited electrons from the dye molecules to the external circuit. Thus, to ensure a high efficiency of electron collection, a fast rate of charge passage is mandatory [69].

For any semiconducting material to function as an ideal photoanode, it must meet these two requirements. Various materials like titanium dioxide, zinc oxide and tin oxide are used as the p-type semiconductor materials [70–72].

TiO_2 has emerged as the primary semiconductor material due to its unique properties which compliment it as a photoanodic material. It is highly abundant, stable and not toxic. A high dielectric constant and a high refractive index elevate TiO_2 among other oxides. Additionally, the specific features listed below make TiO_2 especially suited for DSSCs.

- The mesoporous structure of TiO_2 provides a large surface area to maximize the adsorption of dye molecules [73].
- Because of the internal network structure of TiO_2, the electron collection and transportation is the best in TiO_2 amongst the other oxides [70].
- The energy level of the conduction band edge of TiO_2 is adjustable for electron injection from most of the commercially available dyes.

TiO_2 can be used in many forms like nanoparticles, nanorods, nanoflowers, nanotubes etc. to increase the surface area [74–77]. Mor et al. (in 2005) successfully prepared highly ordered nanotubes of TiO_2, and fabricated a DSSC showing an efficiency of 2.9% [76]. In 2006, Bing Tan and Yiying Wu fabricated a DSSC with TiO_2 nanoparticle and nanowire composite which exhibited an efficiency of 8.6% [77]. Bin Liu and Eray S. Aydil in 2009 introduced a DSSC with a TiO_2 nanorod based photoanode with an efficiency of 3% [75]. In 2013, Jiang et al. used TiO_2 nanoflower clusters as a semiconductor material in a DSSC which exhibited a photoconversion efficiency of 6.38% [74].

1.4.1.1.2 Sensitizer dye

The sensitizer dye is a crucial part of the photoanode as it can absorb sunlight to produce photoexcited electrons. The dye molecules must possess the following properties for them to behave efficiently:

- good photo-stability
- appropriate LUMO level for effective injection of photogenerated electrons into the semiconductor conduction band
- appropriate HOMO level for dye regeneration from the electrolyte, and
- high molar extinction coefficients in the visible and the near-infrared regions for efficient harvesting of sunlight [78].

Ruthenium based sensitizer dyes like di-tetrabutylammonium cis-bis(isothiocyanato)bis(2,2’-bipyridyl-4,4’-dicarboxylato)ruthenium(II) (N719 dye), cis-bis(isothiocyanato) bis(2,2’-bipyridyl-4,4’-dicarboxylato ruthenium(II) (N3 dye) and cis-bis(isothiocyanato)(2,2’-bipyridyl-4,4’-dicarboxylato)(4,4’-di-nonyl-2’-bipyridyl)ruthenium(II)

(Z907 dye) are the most popular amongst all the available dyes [79]. In **Figure 1.15**, the structure of N719 dyes and its corresponding absorption spectrum are shown [80].

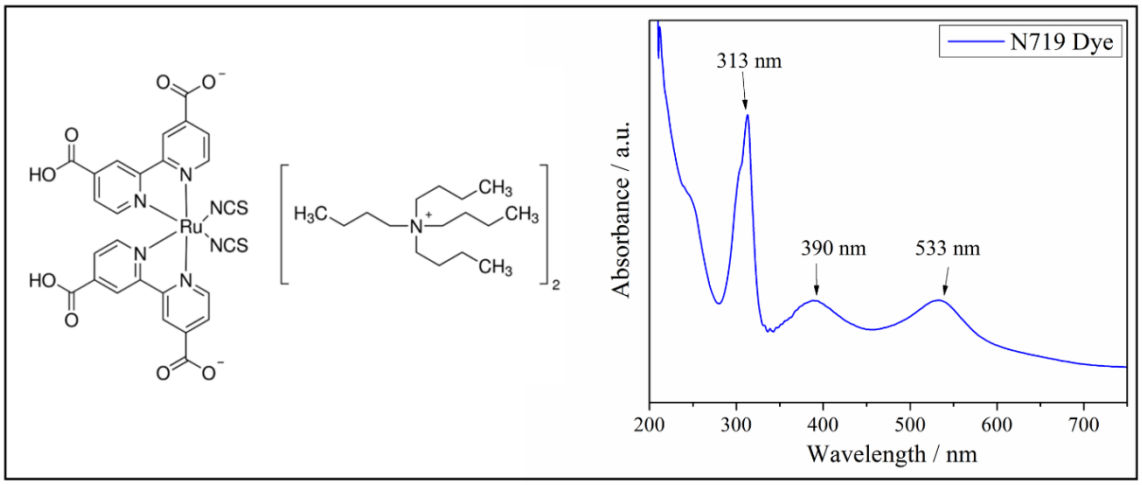

Figure 1.15. Molecular structure and ultraviolet absorption spectrum of N719.

Other categories of sensitizer dyes include:

- **Metal free organic dyes**: alkoxysilyl carbazole**,** dithienopicenocarbazole based low band gap organic dye [81,82].
- **Porphyrin dyes**: donor-π-acceptor zinc porphyrin dye (designated as YD2-*o*-C8) [83].
- **Quantum dot sensitizer dyes**: cadmium-chalcogenide quantum dots, lead-chalcogenide quantum dots and antimony sulfide (Sb_2S_3) quantum dots [84].

1.4.1.2 Counter electrode

Another important component of a DSSC is the counter electrode. It implements two main jobs.

1. It acts as a catalyst to reduce the oxidized ions (triiodide ions) by accepting electrons at the surface of the electrode. If the rate of reduction of the triiodide ions at the counter electrode is fast, it increases the electron flow from the counter electrode to the electrolyte phase. Consequently, higher electric current can be obtained at the outer circuit.
2. It collects electrons from the external load and returns them back into circulation inside the DSSC.

To fulfill these roles the candidates for counter electrode must possess the qualities listed below:

- excellent catalytic activity,
- high electrical conductivity,
- high surface area,

- chemical and electrochemical stability,
- corrosion resistance in the electrolyte environment, and
- matching energy level with the potential of the redox couple in the electrolyte.

Platinum is the best candidate for counter electrode because of its good catalytic activity. Various platinum-free catalysts have also been reported so as to reduce the use of the expensive platinum metal. These include carbon materials like graphene and carbon nanotubes, polymers like polyaniline and PEDOT:PSS, and many others [85–87].

1.4.1.2.1 Platinum

Platinum is the most-preferred counter electrode material for DSSCs [88]. The photoconversion efficiencies exceeding 12% have been realized using platinized counter electrodes [81,83]. The good catalytic activity of platinum towards the reduction of triiodide ions, high conductivity for transport of electrons and its stability makes it superior to other materials. Platinum is used in nanostructures form to increase the surface area as well as the number of catalytic active sites.

Usually a thin layer of platinum on a TCO glass substrate serves as the counter electrode [89,90]. Various techniques and starting materials can be used to prepare platinum counter electrodes. Some of the popular ones include thermal decomposition of chloroplatinic acid (H_2PtCl_6), H_2PtCl_6 reduction by hydrogen, and electrochemical deposition, electron beam evaporation and sputtering of platinum. In 1997, Papageorgiou et al. fabricated platinum counter electrodes on TCO substrates using both thermal decomposition techniques (using H_2PtCl_6 at 380 °C) and electro deposition process. They observed better charge transfer kinetics in the electrode obtained by the thermal decomposition process [91].

Despite its many advantages, platinum also suffers from a few drawbacks.

- It is very expensive. The cost of the counter electrode accounts for ~40% cost of the DSSC.
- It might undergo oxidation and/or dissolution forming platinum(IV) iodide (PtI_4) or iodoplatinic acid (H_2PtI_6) over time in the electrolyte environment containing iodide/triiodide redox couple. Even a tiny amount of platinum, if dissolved in the electrolyte, can re-deposit on the TiO_2 photoanode and catalyse the reduction of triiodide ions, and short-circuit the entire device.
- There is energy mismatch between platinum and electrolytes containing redox couples other than iodide/triiodide, such as cobalt-mediated electrolytes. So it is not very effective in such environments [92–94].

These limitations have led to exploration of platinum-free materials as suitable candidates for counter electrodes.

1.4.1.2.2 Graphene

Graphene is widely used as a counter electrode material in DSSCs because of its outstanding conductivity. The rate of charge transfer kinetics at the counter electrode is immensely increased due to its conductivity. The catalytic activity of graphene is enhanced in the presence of oxygen species or structural defects. These properties can be easily introduced during preparation of graphene. The availability of the raw material (graphite) and easy preparation method make graphene a highly suitable candidate for the platinum-free counter electrode material in DSSC. Additionally, the strong mechanical properties of graphene also provide flexibility to the electrodes.

Graphene as a counter electrode was first studied by Xu et al. in 2008 [95]. A chemically reduced graphene oxide film as the counter electrode was able to show 2.2% photoconversion efficiency. Over the years, the efficiency has improved significantly. Zhang et al. were able to achieve a photoconversion efficiency of 6.81% from the DSSC fabricated with graphene nanosheets counter electrode [96]. Studies have revealed that graphene based catalyst outperforms platinum when cobalt based redox electrolytes are used. While the efficiency with platinum counter electrodes has been limited to ~12% till now, graphene counter electrodes have been found to provide more than 13% efficiency. Mathew et al. used a layer of graphene nanoplatelets on fluorine doped tin oxide (FTO) coated glass as counter electrode and cobalt(II/III) as the redox shuttle, which resulted in a DSSC with an efficiency of 13% [97]. Kakiage et al. also succeeded in obtaining the highest recorded efficiency of 14.3% by using graphene nanoplatelets on gold-treated FTO coated glass substrate as counter electrode and cobalt-mediated electrolyte [94].

1.4.1.2.3 Polyaniline

Another inexpensive material: intrinsically conducting polymer polyaniline shows excellent catalytic activity towards the reduction of triiodide ions, which makes it a suitable candidate for counter electrode. Intrinsically conducting polymers either have metallic conductivity or can act as semiconductors. The electrical properties can be fine-tuned using the methods of organic synthesis and by advanced dispersion techniques. Polyaniline shows high electric conductivity and can be prepared easily from the polymerization of aniline monomer in presence of an oxidant like ammonium persulfate [98].

In 2008, Li et al. first introduced polyaniline as a counter electrode for DSSC [99]. The DSSC was fabricated with microporous polyaniline nanoparticle counter electrode and exhibited an efficiency of 7.15%. To enhance the surface area and numbers of catalytic active sites of polyaniline, it has been prepared as 1-D nanostructures with different morphologies, like nanotubes and nanofibers. In 2015, Park et al. also found that DSSC fabricated with porous

polyaniline nanotube based counter electrode exhibited a photoconversion efficiency of 5.57% [100]. In 2011, Chen et al. introduced a counter electrode based on polyaniline nanofibers/carbon composites for DSSC which showed a photoconversion efficiency of 6.85% under irradiation [101]. The highest efficiency of any polyaniline based counter electrode DSSC was reported by Chiang et al [102]. They prepared the counter electrodes by drop-casting polyaniline/hexafluoro-isopropanol colloid solutions on FTO glass substrate. In iodide/triiodide mediated electrode, they showed an efficiency of 8.8%.

1.4.1.3 Electrolyte

1.4.1.3.1 Liquid electrolyte

The third most important component of a DSSC is the electrolyte. Usually a liquid electrolyte (LE) having a redox couple in an organic solvent is used in DSSCs. The most commonly used combination for LE is iodide/triiodide (I^-/I_3^-) redox couple in an organic solvent mixture of acetonitrile and N-methyl 2-pyrrolidone (NMP), because of its good reversibility and excellent stability. In addition, sometimes additives are also added to the electrolyte to improve the electrochemical properties of the LE. 1-Methyl 3-propylimidazolium iodide (MPI) and t-butyl pyridine (TBP) are two such common additives [103,104].

1.4.1.3.1.1 Solvents

The solvent in the electrolyte provides a medium for the redox couple to carry out the electrochemical processes. Organic solvents are favored to prepare the electrolyte because they can provide a suitable environment in which the ions are easily formed by dissolution of the ionic solutes. The redox ions diffuse from one electrode side to the other *via* the solvent medium. The solvents must possess some important properties in order to become suitable as an electrolyte medium.

- The solvents should have a boiling point above 100 °C so that they remain inside the cell in outdoor conditions.
- They should show adequate chemical stability under light and dark conditions.
- The electrochemical window of the solvent should be wide enough such that no electrochemical degradation occurs at the electrodes within the working potential range.
- The dielectric constant of the solvent should high enough so that sufficient ions are formed by dissociation of the salts in the electrolyte.
- To get a high diffusion of the redox ions, the solvents should have low viscosity.
- The solvents should not absorb visible light.

- They should be chemically inert, and not react with the dye molecules of the photoanode and two electrode materials [105].

Most organic solvents like acetonitrile, NMP, ethylene carbonate and propylene carbonate meet the given requirements. A solvent mixture of acetonitrile and NMP (volume ratio 8:2) is an excellent electrochemical medium in which the triiodide ions can exhibit a higher diffusion coefficient and lower recombination kinetics to achieve a significant efficiency. The addition of NMP in acetonitrile in the mixed solvent improves the long-term stability of the cells due to the low volatility of NMP [106].

1.4.1.3.1.2 Redox couples

The redox couple is the most important component of an electrolyte of DSSC. The two important PV parameters: open-circuit voltage and short-circuit current density are governed by the properties of the redox couple. The magnitude of the open-circuit voltage observed in a DSSC is directly related to the redox potential of the redox couple it is considered as the difference between the Fermi level of the semiconductor photoanode and the redox potential of the redox couple. The open-circuit voltage of a DSSC increases as the redox potential value is closer to the HOMO energy level of the dye molecules. In a DSSC, the reduced state of the redox couple regenerates the oxidized dyes to its original form by undergoing oxidization themselves. To drive this regeneration process, there should be sufficient energy difference between the redox potential of the redox couple and the HOMO level of the dye, otherwise the regeneration process will not occur [107]. Thus, there is a limit of approach of the redox potential to the HOMO level of the dye molecules. Moreover, to achieve a significant current from the device, the oxidized form of the redox couple must diffuse to the counter electrode at a faster rate, and get reduced quickly at the counter electrode. Therefore, the efficiency of a DSSC is directly related the properties of the redox couple used.

Iodide/triiodide redox couple is quite popular as a redox couple for DSSCs because this couple significantly accomplishes the required electrochemical properties mentioned above. Lithium iodide (LiI) and iodine (I_2) are properly dissolved in the solvent to prepare the LE. LiI and I_2 together form the I^-/I_3^- redox couple. The equilibrium state between the iodide and triiodide is shown in the **Eq. (1.3)**.

$$I_3^- + 2e^- \leftrightarrow 3I^- \quad \text{..... (1.3)}$$

And the redox potential of the I^-/I_3^- redox couple is given by the **Eq. (1.4).**

$$E_{redox} = E^{o'} + \frac{RT}{2F} \ln \frac{\left[I_3^-\right]}{\left[I^-\right]} \quad \text{(1.4)}$$

Here, $E^{\circ\prime}$, R, T and F represent the formal potential, gas constant, absolute temperature and Faraday constant respectively.

Cobalt (II/III) redox couple is also frequently used in DSSCs. In 2011, Yella et al. achieved efficiency of 12.3% from a DSSC fabricated with a cobalt (II/III) redox couple based electrolyte [83]. The maximum reported efficiency of any DSSC (14.3%) was also achieved using this redox mediator [94].

1.4.1.3.1.3 Additives

Certain additives are sometimes added to improve the electrochemical properties of the electrolyte. Two additives are worth mentioning here: TBP and MPI. Addition of TBP hinders the recombination processes occurring during the cell operation [108]. In presence of TBP, the conduction band edge of the semiconductor is raised, which increases the magnitude of open-circuit current and fill factor of the DSSC, resulting in enhancement of the photoconversion efficiency [109]. This enhancement is due to the suppression of the recombination reaction between the photoexcited electrons (at the conduction band of the semiconductor) and the triiodide ions present in the electrolyte [110].

An ionic liquid is a salt in molten liquid state, and can be defined as a liquid electrolyte composed exclusively of ions [111]. Ionic liquids like MPI are incorporated in the electrolytes of many DSSCs because of their significant thermal and chemical stability, high ionic conductivity, tunable viscosity, and wide electrochemical potential window [112,113].

1.4.1.3.2 Polymer gel electrolyte

The organic solvents used in the preparation of LE are volatile in nature, thus leakage and evaporation affects the stability of the device. To avoid this problem, scientists are trying to replace the LE with other materials like solid state hole transporting materials or quasi-solid-state electrolytes. Although it is difficult to achieve the same efficiency with these alternative electrolytes at par with the LEs, DSSCs employing these electrolytes show significant durability. Amongst these alternatives, *polymer gel electrolyte* (PGE), also called *quasi-solid-state electrolyte* is drawing huge attention because of its unique electrochemical properties. A polymer material acts as the host in the preparation of the PGE. Some of the host materials include polyethylene oxide, polyethylene glycol, polyacrylic acid, poly(acrylonitrile-co-vinyl acetate), poly(methyl methacrylate), and blend of two or more polymers [114–119].

1.4.1.3.2.1 Poly(methyl methacrylate)

Poly(methyl methacrylate) (PMMA) is used as a polymer host material in PGEs. The preparation process of PMMA is very simple. It entails the free radical polymerization of methyl methacrylate (MMA) in presence of an initiator. PMMA is highly recommended as a polymer host material because of its some interesting properties as listed below.

- The polymer host should not absorb visible light. If the photons required to excite the electrons in the dye molecules are absorbed by the polymer host, then the device will not able to convert the light energy to electricity efficiently. PMMA is optically transparent and does not absorb light in the visible range.
- PMMA is easy to prepare, and readily dissolves in the organic solvent of the LE to form the gel electrolyte.
- The electron rich groups (ester) present in PMMA can restrict the movement of the Li^+ ions present in the electrolyte, resulting in a decrease in the chemical capacitance at the photoanode/electrolyte interface which enhances the open-circuit voltage of the device.

Many PGEs based on PMMA host polymer materials have been investigated and DSSCs with efficiencies exceeding 8% have been achieved [118,120–122]. The DSSCs fabricated with PGEs have exhibited significant stability in comparison to those fabricated with LE under identical experimental conditions [123]. Nevertheless, these cells are faced with two serious problems.

- In a PGE, the medium for the redox couple is in a state of *quasi-solid-state* or *gel state* (i.e. the state between liquid and solid). Such an environment lowers the diffusion process of the redox couples, especially the diffusion kinetics of the bigger ions like the triiodide ions. But, the diffusion processes must follow a very fast route in order to become an efficient photovoltaic device.
- The charge transfer resistances at both the electrode/electrolyte interfaces are higher in devices with PGE, which also negatively affects the current output under irradiation.

Thus, to enhance the efficiency of the durable DSSC fabricated with a PGE, the conditions must be optimized in such a way that the diffusion of triiodide ions in the electrolyte and the charge transfer processes at the interfaces follow a faster route.

1.4.1.3.2.2 Polyaniline

Conducting polymers can be added with a PGE to improve the charge transfer kinetics involved in a quasi-solid-state DSSC. Amongst the many conductive polymers available, polyaniline has great potential to improve the ionic conductivity of a PGE [124,125]. Various PGEs based on polyaniline have been used to fabricate quasi-solid-state DSSCs. In 2012, Tang et

al. introduced a quasi-solid-state DSSC fabricated with a PGE based on poly(acrylic acid)/gelatin/polyaniline composite and the DSSC exhibited a photoconversion efficiency of 6.94% [126]. In 2013, Li et al. achieved a photoconversion efficiency of 6.81% from a quasi-solid-state DSSC fabricated by placing a polyaniline integrated poly(hexamethylene diisocyanate tripolymer/polyethylene glycol) based PGE in between the photoanode and the counter electrode [115]. Surface morphology of polyaniline added in a gel electrolyte also affects the electrochemical behavior of the PGE. Polyaniline can be used in the form of nanotubes, nanofibers, etc. The conductivity of these 1-D materials can be tuned by varying the extent of doping during their synthesis process [127].

1.4.1.3.2.3 Carbon black

Many carbon based conductive nanomaterials like reduced, graphene oxide, graphite powder and carbon nanotubes have been used to prepare composite PGEs to improve their electrochemical properties [128–130]. Carbon black in graphitized form also has potential to become an additive to improve the ionic conductivity of a PGE because of its good conductivity, stability and low cost. In 2006, Ou et al. prepared PMMA/carbon black composites, and studied the electrical conductivities of the composites. They observed that the conductivity of the composites depended on their preparation techniques, and succeeded in obtaining conductivity comparable to that of PMMA/single-wall carbon nanotube composites [131]. Lei et al. (in 2010) fabricated a DSSC with an all-solid-state electrolyte (without iodine) based on carbon black and MPI electrolyte. The fabricated device with optimized amount of carbon black showed an efficiency of 6.37% [132]. In 2010, Lee et al. prepared a quasi-solid-state DSSC by sandwiching an iodine-free electrolyte (based on a polymer electrolyte composed of carbon black loaded polyaniline in an ionic liquid) between a dye sensitized TiO_2 photoanode and a platinum counter electrode. The DSSC exhibited a maximum efficiency of 5.81% [133].

1.4.1.3.2.4 Carbon dots

Different fluorescent materials are used to widen the absorption range of the solar spectrum for maximum harnessing of the solar energy. Yun et al. (in 2015) fabricated a quasi-solid-state DSSC using a PGE with a fluorescent material (4-(dicyanomethylene)-2-methyl-6-(4-dimethylaminostyryl)-4H-pyran). The DSSC with the florescent material exhibited about 1.8% enhancement in efficiency than the DSSC without the florescence material [134]. In 2016, Yao et al. studied the some rare earth ion doped phosphors, and used them in DSSC to widen the absorption range of light. They observed improvement of efficiency in DSSC fabricated with both the up- and down-conversion materials, which converted the infra-red and ultraviolent light into visible light [135]. Since carbon dots also show up-conversion and down-conversion

characteristics, they can be expected to have immense potential to enhance the photoconversion efficiency of a DSSC by widening the sunlight absorption range.

Carbon dots are small fluorescent nanoparticles of carbon with size less than 10 nm [136,137]. They show exceptional properties depending on their structure and composition. Carbon dots are water-soluble because of the carboxyl groups presents on their surface [138]. They have found numerous applications owing to their easy preparation techniques, low cost of the starting materials, good conductivity and fluorescent behavior which can be tuned by surface modification [139–141].

1.4.2 Working principle of DSSCs

The principle of generation of electrical energy in DSSC under irradiation of sunlight can be understood easily by using the schematic energy diagram as shown in **Figure 1.16.** The primary processes occurring inside a DSSC devised using dye sensitized TiO_2 semiconductor photoanode, platinum counter electrode and iodide/triiodide redox couple mediated electrolyte are symbolized with the numbers **(1)-(6)**. The scale shown in the left side of the energy level diagram represents the potentials with respect to standard calomel electrode (SCE). The processes are explained as follows:

(1) Under irradiation of sunlight, the incident photons with specific energies excite electrons from the HOMO level to the LUMO level of the dye molecules (adsorbed on TiO_2). The intensity of the incident light with proper energy determines the population of the photoexcited electrons at the LUMO level of the dyes. The typical lifetime of the electrons at the LUMO level of the dye molecules is in femtosecond timescale.

(2) The photoexcited electrons are rapidly injected into the conduction band of TiO_2, and they subsequently diffuse to the TCO glass sheet.

(3) The iodide/triiodide redox couple present in the electrolyte plays the next step. The iodide ions reduce the oxidized dye molecules to their initial state, and themselves get oxidized to triiodide ions.

(4) In the next step, triiodide ions get reduced to iodide ions at the counter electrode. The reduction is facilitated by the electrons collected at the counter electrode coming from the outer circuit.

During these four processes, involvement of photon and electron occurs without any consumption of physical material. These processes contribute to the generation of electrical energy under irradiation of light and are known as *forward processes* or *forward reactions*. However, along with these processes, some other processes also occur in the cell which lower the number of collected electrons at the photoanode and hamper the quality of the cell. These

reactions are termed as *dark processes* or *dark reactions*. Processes **(5)** and **(6)** represent the two dark processes involved in the DSSC.

(5) The photoexcited electrons in the conduction band of TiO_2 can go back to the vacant HOMO of the dye particles.

(6) The photoexcited electrons can also take part in the reduction of triiodide ions to iodide ions.

These two processes decrease the magnitude of the output electric current in a cell. The regeneration kinetics of the oxidized dye molecules by iodide ions must follow a faster reaction kinetic (nanoseconds scale) to compete with the two recombination process. Otherwise, the cell efficiency becomes low.

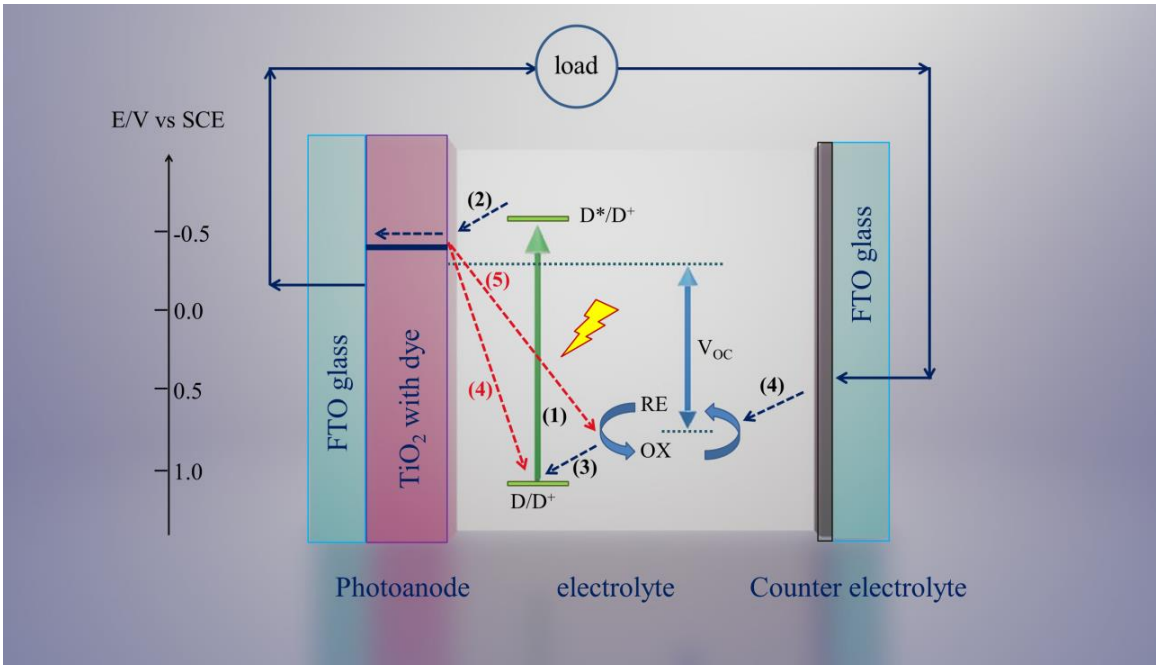

Figure 1.16. Processes involved during the working of a typical DSSC under light.

The processes involved during this photovoltaic operation under light can also be expressed by equations as follows:

$$D\,|\,TiO_2 + h\nu \rightarrow D^*\,|\,TiO_2 \qquad \text{(a)}$$

$$D^*\,|\,TiO_2 \rightarrow D^+\,|\,TiO_2 + e_{cb}^-\left(TiO_2\right) \qquad \text{(b)}$$

$$D^+\,|\,TiO_2 + 3I^- \rightarrow D\,|\,TiO_2 + I_3^- \qquad \text{(c)}$$

$$I_3^- + Pt \rightarrow 3I^- \qquad \text{(d)}$$

$$e_{cb}^{-}\left(TiO_2\right)+D^{+}\,|\,TiO_2 \rightarrow D\,|\,TiO_2 \qquad \text{(e)}$$

$$e_{cb}^{-}\left(TiO_2\right)+3I^{-} \rightarrow I_3^{-} \qquad \text{(f)}$$

Dye molecule is denoted as D and its excited state is represented by D*. **Eq. (a)** represents the process **(1)** involved in the cell. The dye molecule adsorbed on TiO_2 (D | TiO_2) gets excited to D* | TiO_2 by absorbing photon energy of *hv* (*h* and *v* are the Plank constant and frequency respectively). **Eq. (b)** shows the injection of the excited electrons from the D* | TiO_2 to the conduction band of the TiO_2 ($e_{cb}^{-}\left(TiO_2\right)$), leaving behind holes in the dye molecule (D^{+} | TiO_2). The regeneration of the oxidized dye molecule by iodide ions is expressed in the **Eq. (c)**. **Eq. (d)** shows the reduction process of the triiodide ion to iodide ions involved at the platinum counter electrode. The recombination processes occurring in the DSSC are expressed in **Eqs. (e)** and **(f)**. The electrons in the TiO_2 conduction band ($e_{cb}^{-}\left(TiO_2\right)$) can either recombine with the hole generated in the HOMO level of the dye (Eq. (e)), or can reduce triiodide ions present close to the photoanode (Eq. (f)).

1.5 Solar cell performance parameters

A typical p-n junction solar cell is similar to a diode model, and can be represented by using an equivalent circuit model as shown in **Figure 1.17** [142]. The net current generated under the irradiation of light by this solar cell is defined by the **Eq. (1.7)**

$$I = I_L - I_D \qquad \textbf{(1.5)}$$

$$I_D = I_o\left(e^{qV/kT} - 1\right) \qquad \textbf{(1.6)}$$

$$I = I_L - I_o\left(e^{qV/kT} - 1\right) \qquad \textbf{(1.7)}$$

Here, *I*, I_L, I_D, I_O, *q*, *V*, *k* and *T* represent net current, photogenerated current, diode current, dark saturation current (or reverse saturation current because of the recombination in space charge regions), charge, voltage, Boltzmann constant and temperature respectively.

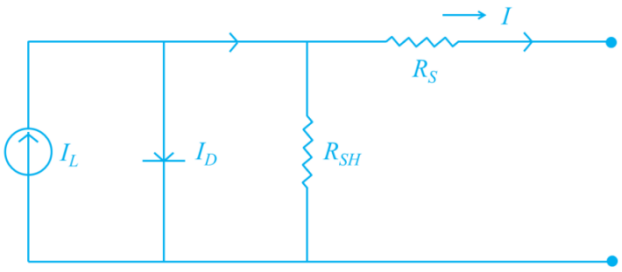

Figure 1.17. Circuit diagram of a solar cell.

A diode current is observed in the cell due to the fact that it acts like a forward bias diode under irradiation of light. The photogenerated current is usually higher in magnitude than the diode current, and flows in the opposite direction. The last term in the **Eq. (1.7)** represents the diode current which is derived from Shockley diode equation (**Eq. (1.6)**). In addition to these current components, two inevitable resistive components are always present in a cell as shown in the equivalent circuit diagram. Consequently, the solar cell current-voltage (*I-V*) characteristic equation (derived by using minority carrier diffusion) includes the parasitic series (R_S) and shunt (R_{SH}) resistances, and is finally expressed as **Eq. (1.8)**

$$I = I_L - I_o\left(e^{q(V+IR_S)/kT} - 1\right) - \frac{V + IR_S}{R_{SH}} \quad \text{..... (1.8)}$$

It follows from the **Eq. (1.8)** that at a low applied voltage, the current through the diode is very small and almost equal to the short circuit current (photogenerated current at V=0). At higher voltage, the recombination current at the diode becomes significant, resulting in a rapid decrease of the output current. A typical *I-V* characteristic curve for a solar cell is shown in **Figure 1.18.**

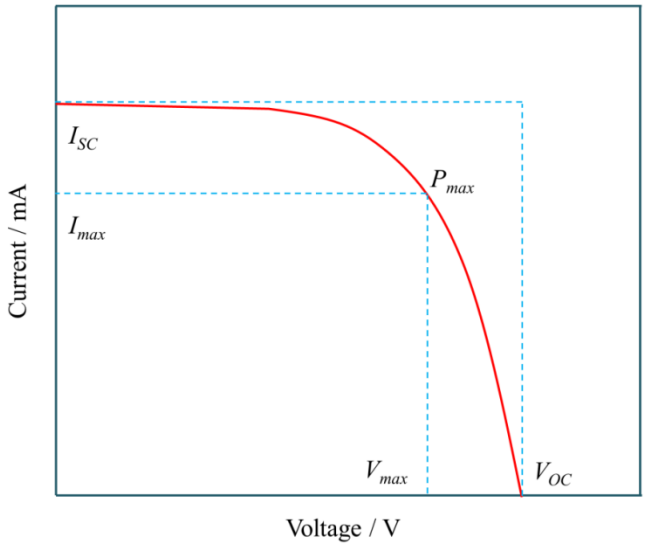

Figure 1.18. *I-V* characteristic curve of a solar cell under illumination of light.

The performance quality of a solar cell can be obtained by calculating some figures of merit from the *I-V* characteristic plot under irradiation. They include open-circuit voltage (V_{OC}), short-circuit current (I_{SC}) and fill factor (*FF*).

- **Short circuit current**: I_{SC} is the current obtained from the *I-V* characteristic plot at zero applied potential, or in other words it is the current at zero load resistance. Usually the term short-circuit current density (J_{SC}) is more commonly used. This current density is obtained by dividing the I_{SC} with the effective area of the solar cell. The magnitude of the J_{SC} primarily depends upon the intensity of the solar irradiance, properties of the semiconductor material used and the charge transfer resistances of the cell.
- **Open-circuit voltage**: V_{OC} is the highest voltage observed in a solar cell at infinite resistance load. In other words, V_{OC} represents the voltage of the cell at zero I_{SC} in the *I-V* characteristic plot. The corresponding voltage and current at the maximum power point in the *I-V* curve are known as maximum voltage (V_{max}) and maximum current density (J_{max}).
- **Fill factor:** It represents the squareness of the curve, i.e., it signifies the maximum power output from a PV cell. The magnitude of R_{SH} and R_S greatly affects the shape and squareness of the *I-V* characteristic curve. The values of V_{OC} and J_{max} reduce in the presence of R_{SH}, while I_{SC} remains unaffected. On the other hand, a decrease in R_S increases J_{SC} and V_{max} without affecting the value of V_{OC} [143,144]. **Figure 1.19** exhibits the effect of the two resistances on the shape of the *I-V* characteristic plot. The squareness of the *I-V* plot is higher at lower values of R_{SH} and R_S.

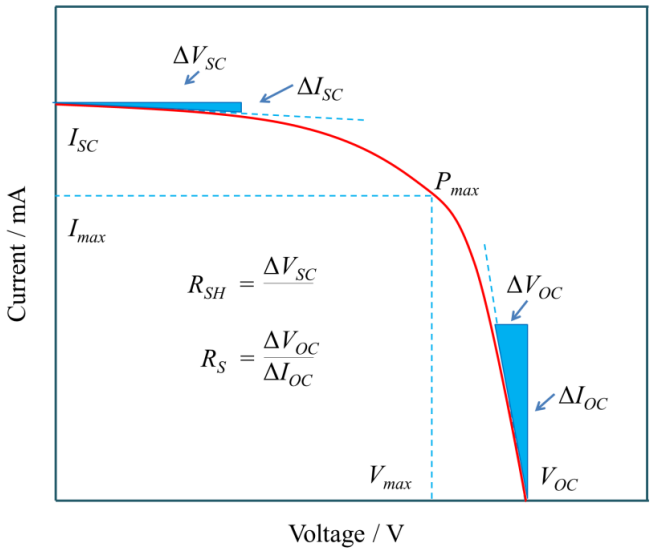

Figure 1.19. Effect of resistances on the shape of the *I-V* characteristic plot.

FF is mathematically expressed as follows:

$$FF = \frac{V_{\max} \times I_{\max}}{V_{oc} \times I_{sc}} \quad \text{.....} \quad \textbf{(1.9)}$$

Finally the **efficiency** (η) of a solar cell is mathematically expressed as:

$$\eta = \frac{V_{oc} \times I_{sc} \times FF}{P_{in}} \quad \text{……..……..... (1.10)}$$

where P_{in} is the power of the incident light, usually the value of it is 1000 W m^{-2}.

1.5.1 Device parameters of DSSCs

Device parameters of a solar cell are developed from their *I-V* characteristic or *J-V* characteristic plots. DSSCs also have the same device parameters as the conventional p-n junction solar cells like J_{SC}, V_{OC}, *FF* and efficiency.

DSSC is also called a photo-electrochemical cell because along with the device physics, electrochemistry is also involved in a DSSC. The electrochemical study of the electrolyte, mainly the electrochemical behavior of the redox couple in the electrolyte is important since its redox potential plays a key role in determining the value of V_{OC} of the device under irradiation. The V_{OC} of a DSSC is the difference between the energy of the quasi-Fermi level of the semiconductor (E_F) and the redox potential (E_{redox}) of the redox couple present in the electrolyte. Mathematically, V_{OC} can be represented as the **Eq. (1.11)**

$$qV_{oc} = E_F - E_{redox} \text{ ….……..…….. (1.11)}$$

where q is the charge. E_F can be mathematically expressed as **Eq. (1.12)**

$$E_F = E_c + kT \ln \frac{n_c}{N_c} \text{ …...……..……...…… (1.12)}$$

where E_C, k, T, n_c and N_C represent the conduction band edge of the semiconductor, Boltzmann constant, temperature, density of free electron at the conduction band of the semiconductor and density of accessible state of the semiconductor's conduction band respectively. Thus, the general mathematical expression of V_{OC} of a DSSC under irradiation is as shown in the **Eq. (1.13)**

$$V_{oc} = \frac{kT}{q}\left(\frac{E_c - E_{redox}}{kT} + \ln \frac{n_c}{N_c}\right) \text{ ……...……..……. (1.13)}$$

In this relation, E_C, n_C and N_C are the only variables, the other terms including the redox potential is fixed d for a particular redox couple. Thus, the magnitude of V_{OC} is varied only because of these three variables.

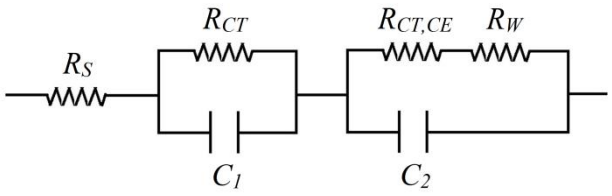

Figure 1.20. Equivalent circuit diagram of the resistances of a typical DSSC.

A higher value of V_{OC} enhances the electric current flow in the outer circuit. But the magnitude of the current is negatively impacted by many factors like the inevitable resistance components and the recombination processes involved in the cell. An equivalent circuit as shown in the **Figure 1.20** is used to represent the resistive components of a DSSC. R_S, R_{CT}, $R_{CT,CE}$ and R_W are the series resistance, the charge transfer resistance at the electrolyte/photoanode interface, the charge transfer resistance at the electrolyte/counter electrode interface and the Warburg impedance due to the diffusion of the triiodide ions respectively. These resistances are inevitable but can be minimized in a DSSC to draw the maximum possible current. Two capacitive components C_1 and C_2 are also observed at both the electrode/electrolyte interfaces because of the ions present in the electrolyte composition.

1.6 Objectives

Economically, DSSCs are advantageous due to their low fabrication cost. But efficiency of these devices is less as compared to silicon based devices. DSSCs having efficiency of 13-14% have been achieved by researchers. So, it has a great potential to equally compete with other solar cells. However, the leakage of the electrolyte often negatively affects the durability and efficiency of the DSSC. Efforts are made to improve the cell's durability by replacing the liquid electrolyte with a polymer based gel electrolyte. Furthermore, the high cost of platinum counter electrode has also spearheaded the search for alternative cheap options for counter electrodes. A detailed study of the polymer gel electrolytes and alternate counter electrodes provides a direction in progress of improving the durability and cost-effectiveness of the DSSC without compromising the output efficiency.

The main objectives of this research work include:

1. Synthesis of different PMMA based polymer gel electrolytes with tailor-made properties like high conductivity and broadening the sunlight absorption region.
2. Synthesis of graphene based polyaniline nanotube aerogel counter electrode as low-cost platinum-free counter electrode.
3. Study of the electrochemical behavior of the gel electrolytes and the counter electrodes.
4. Fabrication and optimization of quasi-solid-state DSSCs using the prepared components.

1.7 Plan of research work

To accomplish the objectives, the following methodologies will be implemented.

1.7.1 Preparation of gel electrolytes

To obtain the PMMA based PGEs, the following steps will be adopted.

- Synthesis of PMMA by using a free radical polymerization of MMA monomer in the presence of benzoyl peroxide initiator.
- Synthesis of polyaniline nanotubes by chemical oxidation polymerization of aniline in the presence of ammonium persulfate oxidant and oxalic acid.
- Synthesis of green emitting carbon dots using a solid-state reaction of diamonium hydrogen citrate and urea at high temperature.
- Preparation of three different PMMA based polymer composites by varying weight percentages of the fillers:
    1. PMMA/polyaniline nanotube composite,
    2. PMMA/carbon black composite, and
    3. PMMA/carbon dot composite.
- Preparation of polymer gel electrolytes incorporating the three composites.

1.7.2 Preparation of counter electrode

The following steps will be followed to obtain the platinum-free counter electrode.

- Synthesis of graphene oxide by using modified Hummers method.
- Synthesis of polyaniline nanotube/reduced graphene oxide aerogel by resorcinol−formaldehyde solution initiated polymerization technique, followed by freeze-drying.

1.7.3 Characterization of the materials

- The as-synthesized materials will be characterized using different analytical tools, such as Fourier transform infra-red spectroscopy, UV-visible spectroscopy, fluorescence spectroscopy, X-ray diffraction, Raman spectroscopy, X-ray photoelectron spectroscopy, scanning electron microscopy and transmission electron microscopy, etc.

1.7.4 Fabrication of the devices

- Fabrication of three different quasi-solid-state DSSCs with PMMA/polyaniline nanotube, PMMA/carbon black and PMMA/carbon dot PGEs.
- Fabrication of a quasi-solid-state DSSC with platinum-free polyaniline nanotube/reduced graphene oxide aerogel based counter electrode.

1.7.5 Electrochemical tests of the devices

- The electrochemical performance of the fabricated DSSCs will be evaluated using tools such as *J-V* characteristic plots, electrochemical impedance spectroscopy, cyclic voltammetry and Tafel plots, etc. under irradiation of AM 1.5 (100 mW cm^{-2}) light generated from a solar simulator.
- Investigation of the long-term stability of the fabricated devices by recording device parameters upto 1000 hours.

1.8 References

[1] Banos, R., Manzano-Agugliaro, F., Montoya, F. G., Gil, C., Alcayde, A., and Gómez, J. Optimization methods applied to renewable and sustainable energy: A review. *Renewable and Sustainable Energy Reviews*, 15(4):1753-1766, 2011.

[2] Apergis, N. and Payne, J. E. Renewable and non-renewable energy consumption-growth nexus: Evidence from a panel error correction model. *Energy Economics*, 34(3):733-738, 2012.

[3] El Chaar, L., lamont, L. A., and El Zein, N. Review of photovoltaic technologies. *Renewable and Sustainable Energy Reviews*, 15(5):2165-2175, 2011.

[4] Grätzel, M. Solar energy conversion by dye-sensitized photovoltaic cells. *Inorganic Chemistry*, 44(20):6841-6851, 2005.

[5] Pagliaro M., Palmisano G., and Ciriminna, R. *Flexible solar cells.* Wiley-VCH, Weinheim, Germany, 2008.

[6] Solanki, C. S. *Solar photovoltaics : fundamentals, technologies and applications*. PHI Learning Private Limited, 3rd edition, 2015.

[7] Smith, W. Effect of light on selenium during the passage of an electric current. *Nature*, 7(173):303, 1873.

[8] Chapin, D. M., Fuller, C. S., and Pearson, G. L. A new silicon p-n junction photocell for converting solar radiation into electrical power. *Journal of Applied Physics*, 25(5):676-677, 1954.

[9] PVPS, I. 2018 Snapshot of Global Photovoltaic Markets. IEA PVPS T1-33, 2018.

[10] Shockley, W. and Queisser, H. J. Detailed balance limit of efficiency of p-n junction solar cells. *Journal of Applied Physics*, 32(3):510-519, 1961.

[11] Rühle, S. Tabulated values of the Shockley-Queisser limit for single junction solar cells. *Solar Energy*, 130:139-147, 2016.

[12] Zweibel, K., Mason, J., and Fthenakis, V. A solar grand plan. *Scientific American*, 298(1):64-73, 2008.

[13] Shah, A., Torres, P., Tscharner, R., Wyrsch, N., and Keppner, H. Photovoltaic technology: The case for thin-film solar cells. *Science*, 285(5428):692-698, 1999.

[14] Bag, S., Gunawan, O., Gokmen, T., Zhu, Y., Todorov, T. K., and Mitzi, D. B. Low band gap liquid-processed CZTSe solar cell with 10.1% efficiency. *Energy and Environmental Science*, 5(5):7060-7065, 2012.

[15] Katagiri, H., Jimbo, K., Maw, W. S., Oishi, K., Yamazaki, M., Araki, H., and Takeuchi, A. Development of CZTS-based thin film solar cells. *Thin Solid Films*, 517(7):2455-2460, 2009.

[16] Guo, Q., Ford, G. M., Yang, W. C., Walker, B. C., Stach, E. A., Hillhouse, H. W. and Agrawal, R. Fabrication of 7.2% efficient CZTSSe solar cells using CZTS nanocrystals. *Journal of the American Chemical Society*, 132(49):17384-17386, 2010.

[17] Cheng, Y. J., Yang, S. H., and Hsu, C. S. Synthesis of conjugated polymers for organic solar cell applications. *Chemical Reviews*, 109(11):5868-5923, 2009.

[18] Gong, J., Liang, J., and Sumathy, K. Review on dye-sensitized solar cells (DSSCs): Fundamental concepts and novel materials. *Renewable and Sustainable Energy Reviews*, 16(8):5848-5860, 2012.

[19] Kamat, P. V. Quantum dot solar cells. Semiconductor nanocrystals as light harvesters. *Journal of Physical Chemistry C*, 112(48):18737-18753, 2008.

[20] Niu, G., Guo, X., and Wang, L. Review of recent progress in chemical stability of perovskite solar cells. *Journal of Materials Chemistry A*, 3(17):8970-8980, 2015.

[21] Green, M. A. *Crystalline Silicon Solar Cells*. 1954.

[22] Kayes, B. M., Atwater, H. A., and Lewis, N. S. Comparison of the device physics principles of planar and radial p-n junction nanorod solar cells. *Journal of Applied Physics*, 97(11):114302, 2005.

[23] Müller, A., Ghosh, M., Sonnenschein, R., and Woditsch, P. Silicon for photovoltaic applications. *Materials Science and Engineering: B*, 134(2-3):257-262, 2006.

[24] Carlberg, T., King, T. B., and Witt, A. F. Dynamic oxygen equilibrium in silicon melts during crystal growth by the Czochralski technique. *Journal of the Electrochemical Society*, 129(1):189, 1982.

[25] Abrosimov, N. V., Rossolenko, S. N., Alex, V., Gerhardt, A., and Schröder, W. Single crystal growth of $Si_{1-x}Ge_x$ by the Czochralski technique. *Journal of Crystal Growth*, 166(1-4):657-662, 1996.

[26] Hahn, G. and Schönecker, A. New crystalline silicon ribbon materials for photovoltaics. *Journal of Physics Condensed Matter*, 16(50):R1615-R1648, 2004.

[27] Fujiwara, K., Pan, W., Usami, N., Sawada, K., Tokairin, M., Nose, Y., Nomura, A., Shishido, T., and Nakajima, K. Growth of structure-controlled polycrystalline silicon ingots for solar cells by casting. *Acta Materialia*, 54(12):3191-3197, 2006.

[28] Franke, D., Rettelbach, T., Häßler, C., Koch, W., and Müller, A. Silicon ingot casting: Process development by numerical simulations. *Solar Energy Materials and Solar Cells*, 72(1-4):83-92, 2002.

[29] Saga, T. Advances in crystalline silicon solar cell technology for industrial mass production. *NPG Asia Materials*, 2(3):96-102, 2010.

[30] Aberle, A. G. Thin-film solar cells. *Thin Solid Films*, 517(17):4706-4710, 2009.

[31] Bloss, W. H., Pfisterer, F., Schubert, M., and Walter, T. Thin-film solar cells. *Progress in*

Photovoltaics: Research and Applications, 3(1):3-24, 1995.

[32] Chopra, K. L. and Das, S. R. Why thin film solar cells? *Thin Film Solar Cells*, pages 1-18, ISBN:978-1-4899-0418-8. Springer US, Boston, MA, 1983.

[33] Garnett, E. C. and Yang, P. Silicon nanowire radial p−n junction solar cells. *Journal of the American Chemical Society*, 130(29):9224-9225, 2008.

[34] Bergmann, R. B. Crystalline Si thin-film solar cells: A review. *Applied Physics A: Materials Science and Processing*, 69(2):187-194, 1999.

[35] Dennler, G., Scharber, M. C., and Brabec, C. J. Polymer-fullerene bulk-heterojunction solar cells. *Advanced Materials*, 21(13):1323-1338, 2009.

[36] Yan, B., Yue, G., Sivec, L., Yang, J., Guha, S., and Jiang, C. S. Innovative dual function nc-SiO_x:H layer leading to a > 16% efficient multi-junction thin-film silicon solar cell. *Applied Physics Letters*, 99(11):113512, 2011.

[37] Green, M. A. Thin-film solar cells: Review of materials, technologies and commercial status. *Journal of Materials Science: Materials in Electronics*, 18(SUPPL. 1):15-19, 2007.

[38] Ramanathan, K., Contreras, M. A., Perkins, C. L., Asher, S., Hasoon, F. S., Keane, J., Young, D., Romero, M., Metzger, W., Noufi, R., and Ward, J. Properties of 19.2% efficiency ZnO/CdS/$CuInGaSe_2$ thin-film solar cells. *Progress in Photovoltaics: Research and Applications*, 11(4):225-230, 2003.

[39] Britt, J. and Ferekides, C. Thin-film CdS/CdTe solar cell with 15.8% efficiency. *Applied Physics Letters*, 62(22):2851-2852, 1993.

[40] Romeo, N., Bosio, A., Canevari, V., and Podestà, A. Recent progress on CdTe/CdS thin film solar cells. *Solar Energy*, 77(6):795-801, 2004.

[41] Jackson, P., Hariskos, D., Lotter, E., Paetel, S., Wuerz, R., Menner, R., Wischmann, W., and Powalla, M. New world record efficiency for Cu(In,Ga)Se_2 thin-film solar cells beyond 20%. *Progress in Photovoltaics: Research and Applications*, 19(7):894-897, 2011.

[42] Gregg, B. A. The photoconversion mechanism of excitonic solar cells. *MRS Bulletin*, 30(1):20-22, 2005.

[43] Choi, J. J., Lim, Y. F., Santiago-Berrios, M. E. B., Oh, M., Hyun, B. R., Sun, L., Bartnik, A. C., Goedhart, A., Malliaras, G. G., Abruna, H. D., and Wise, F. W. PbSe nanocrystal excitonic solar cells. *Nano Letters*, 9(11):3749-3755, 2009.

[44] Giebink, N. C., Wiederrecht, G. P., Wasielewski, M. R., and Forrest, S. R. Thermodynamic efficiency limit of excitonic solar cells. *Physical Review B:Condensed Matter and Materials Physics*, 83(19):195326, 2011.

[45] Gonzalez-Valls, I. and Lira-Cantu, M. Vertically-aligned nanostructures of ZnO for excitonic solar cells: A review. *Energy and Environmental Science*, 2(1):19-34, 2009.

[46] Gregg, B. A. Excitonic solar cells. *The Journal of Physical Chemistry B*, 107(20):4688-

4698, 2003.

[47] Gregg, B. A. and Hanna, M. C. Comparing organic to inorganic photovoltaic cells: Theory, experiment, and simulation. *Journal of Applied Physics*, 93(6):3605-3614, 2003.

[48] Gregg, B. A. The photoconversion mechanism of excitonic solar cells. *MRS Bulletin*, 30(1):20-22, 2005.

[49] Chen, C. C., Chang, W. H., Yoshimura, K., Ohya, K., You, J., Gao, J., Hong, Z., and Yang, Y. An efficient triple-junction polymer solar cell having a power conversion efficiency exceeding 11%. *Advanced Materials*, 26(32):5670-5677, 2014.

[50] Hiramoto, M., Fujiwara, H., and Yokoyama, M. Three-layered organic solar cell with a photoactive interlayer of codeposited pigments. *Applied Physics Letters*, 58(10):1062-1064, 1991.

[51] Aernouts, T., Vanlaeke, P., Geens, W., Poortmans, J., Heremans, P., Borghs, S., Mertens, R., Andriessen, R., and Leenders, L. Printable anodes for flexible organic solar cell modules. *Thin Solid Films*, 451-452:22-25, 2004.

[52] Zhou, H., Yang, L., Stuart, A. C., Price, S. C., Liu, S., and You, W. Development of fluorinated benzothiadiazole as a structural unit for a polymer solar cell of 7% efficiency. *Angewandte Chemie International Edition*, 50(13):2995-2998, 2011.

[53] Verreet, B., Rand, B. P., Cheyns, D., Hadipour, A., Aernouts, T., Heremans, P., Medina, A., Claessens, C. G., and Torres, T. A 4% efficient organic solar cell using a fluorinated fused subphthalocyanine dimer as an electron acceptor. *Advanced Energy Materials*, 1(4):565-568, 2011.

[54] O'Regan, B. and Grätzel, M. A low-cost, high-efficiency solar cell based on dye-sensitized colloidal TiO_2 films. *Nature*, 353(6346):737-740, 1991.

[55] Gerischer, H., Michel-Beyerle, M. E., Rebentrost, F., and Tributsch, H. Sensitization of charge injection into semiconductors with large band gap. *Electrochimica Acta*, 13(6):1509-1515, 1968.

[56] Tributsch, H. and Calvin, M. Electrochemistry of excited molecules: photo-electrochemical reactions of chlorophylls. *Photochemistry and Photobiology*, 14(2):95-112, 1971.

[57] Tributsch, H. Reaction of excited chlorophyll molecules at electrodes and in photosynthesis. *Photochemistry and Photobiology*, 16(4):261-269, 1972.

[58] Murray, C. B., Kagan, C. R., and Bawendi, M. G. Synthesis and characterization of monodisperse nanocrystals and close-packed nanocrystal assemblies. *Annual Review of Materials Science*, 30(1):545-610, 2000.

[59] Lan, X., Voznyy, O., García de Arquer, F. P., Liu, M., Xu, J., Proppe, A. H., Walters, G., Fan, F., Tan, H., Liu, M., and Yang, Z. 10.6% Certified colloidal quantum dot solar cells

via solvent-polarity-engineered halide passivation. *Nano Letters*, 16(7):4630-4634, 2016.

[60] Collavini, S., Völker, S. F., and Delgado, J. L. Understanding the outstanding power conversion efficiency of perovskite-based solar cells. *Angewandte Chemie International Edition*, 54(34):9757-9759, 2015.

[61] Kojima, A., Teshima, K., Shirai, Y., and Miyasaka, T. Organometal halide perovskites as visible-light sensitizers for photovoltaic cells. *Journal of the American Chemical Society*, 131(17):6050-6051, 2009.

[62] Xiao, Z., Bi, C., Shao, Y., Dong, Q., Wang, Q., Yuan, Y., Wang, C., Gao, Y., and Huang, J. Efficient, high yield perovskite photovoltaic devices grown by interdiffusion of solution-processed precursor stacking layers. *Energy Environ. Sci.*, 7(8):2619-2623, 2014.

[63] Mei, A., Li, X., Liu, L., Ku, Z., Liu, T., Rong, Y., Xu, M., Hu, M., Chen, J., Yang, Y., and Grätzel, M. A hole-conductor-free, fully printable mesoscopic perovskite solar cell with high stability. *Science (New York, N.Y.)*, 345(6194):295-298, 2014.

[64] Eames, C., Frost, J. M., Barnes, P. R., O'regan, B. C., Walsh, A., and Islam, M. S. Ionic transport in hybrid lead iodide perovskite solar cells. *Nature Communications*, 6(1):7497, 2015.

[65] Kojima, A., Teshima, K., Shirai, Y., and Miyasaka, T. Organometal halide perovskites as visible-light sensitizers for photovoltaic cells. *Journal of the American Chemical Society*, 131(17):6050-6051, 2009.

[66] Lee, M. M., Teuscher, J., Miyasaka, T., Murakami, T. N., and Snaith, H. J. Efficient hybrid solar cells based on meso-superstructured organometal halide perovskites. *Science*, 338(6107):643-647, 2012.

[67] *National Renewable Energy Laboratory, Best Research-Cell Efficiencies*. Retrieved on 25 Apr. 2018 from https://www.nrel.gov/pv/assets/pdfs/pv-efficiencies-07-17-2018.pdf, 2016.

[68] Peter, L. Transport, trapping and interfacial transfer of electrons in dye-sensitized nanocrystalline solar cells. *Journal of Electroanalytical Chemistry*, 599(2):233-240, 2007.

[69] Maçaira, J., Andrade, L., and Mendes, A. Review on nanostructured photoelectrodes for next generation dye-sensitized solar cells. *Renewable and Sustainable Energy Reviews*, 27:334-349, 2013.

[70] Grätzel, M. Dye-sensitized solar cells. *Journal of Photochemistry and Photobiology C: Photochemistry Reviews*, 4(2):145-153, 2003.

[71] Wu, J. J., Chen, G. R., Yang, H. H., Ku, C. H., and Lai, J. Y. Effects of dye adsorption on the electron transport properties in ZnO-nanowire dye-sensitized solar cells. *Applied Physics Letters*, 90(21):213109, 2007.

[72] Gubbala, S., Chakrapani, V., Kumar, V., and Sunkara, M. K. Band-edge engineered hybrid structures for dye-sensitized solar cells based on SnO_2 nanowires. *Advanced Functional*

Materials, 18(16):2411-2418, 2008.

[73] Wang, Z. S., Kawauchi, H., Kashima, T., and Arakawa, H. Significant influence of TiO_2 photoelectrode morphology on the energy conversion efficiency of N719 dye-sensitized solar cell. *Coordination Chemistry Reviews*, 248(13-14):1381-1389, 2004.

[74] Jiang, Y., Li, M., Ding, R., Song, D., Trevor, M., and Chen, Z. Enhanced the performance of dye-sensitized solar cells with a novel photoanode using TiO_2 nanoflower clusters and nanoparticles. *Materials Letters*, 107:210-213, 2013.

[75] Liu, B. and Aydil, E. S. Growth of oriented single-crystalline rutile TiO_2 nanorods on transparent conducting substrates for dye-sensitized solar cells. *Journal of the American Chemical Society*, 131(11):3985-3990, 2009.

[76] Mor, G. K., Shankar, K., Paulose, M., Varghese, O. K., and Grimes, C. A. Use of highly-ordered TiO_2 nanotube arrays in dye-sensitized solar cells. *Nano Letters*, 6(2):215-218, 2006.

[77] Tan, B. and Wu, Y. Dye-sensitized solar cells based on anatase TiO_2 nanoparticle/nanowire composites. *Journal of Physical Chemistry B*, 110(32):15932-15938, 2006.

[78] Zhang, S., Yang, X., Numata, Y., and Han, L. Highly efficient dye-sensitized solar cells: Progress and future challenges. *Energy and Environmental Science*, 6(6):1443-1464, 2013.

[79] Gong, J., Liang, J., and Sumathy, K. Review on dye - sensitized solar cells (DSSCs) : Fundamental concepts and novel materials. *Renewable and Sustainable Energy Reviews*, 16(8):5848-5860, 2012.

[80] Wang, Z.S., Kawauchi, H., Kashima, T., and Arakawa, H. Significant influence of TiO_2 photoelectrode morphology on the energy conversion efficiency of N719 dye-sensitized solar cell. *Coordination Chemistry Reviews*, 248(13-14):1381-1389, 2004.

[81] Kakiage, K., Aoyama, Y., Yano, T., Otsuka, T., Kyomen, T., Unno, M., and Hanaya, M. An achievement of over 12 percent efficiency in an organic dye-sensitized solar cell. *Chemical Communications*, 50(48):6379-6381, 2014.

[82] Yao, Z., Wu, H., Li, Y., Wang, J., Zhang, J., Zhang, M., Guo, Y. and Wang, P. Dithienopicenocarbazole as the kernel module of low-energy-gap organic dyes for efficient conversion of sunlight to electricity. *Energy & Environmental Science*, 8(11):3192-3197, 2015.

[83] Yella, A., Lee, H. W., Tsao, H. N., Yi, C., Chandiran, A. K., Nazeeruddin, M. K., Diau, E. W. G., Yeh, C. Y., Zakeeruddin, S. M., and Grätzel, M. Porphyrin-sensitized solar cells with cobalt (II/III)-based redox electrolyte exceed 12 percent efficiency. *Science*, 334(6056):629-634, 2011.

[84] Rhee, J. H., Chung, C.-C., and Diau, E. W.-G. A perspective of mesoscopic solar cells

based on metal chalcogenide quantum dots and organometal-halide perovskites. *NPG Asia Materials*, 5(10):e68, 2013.

[85] Yoon, C. H., Vittal, R., Lee, J., Chae, W. S., and Kim, K. J. Enhanced performance of a dye-sensitized solar cell with an electrodeposited-platinum counter electrode. *Electrochimica Acta*, 53(6):2890-2896, 2008.

[86] Roy-Mayhew, J. D., Bozym, D. J., Punckt, C., and Aksay, I. A. Functionalized graphene as a catalytic counter electrode in dye-sensitized solar cells. *ACS Nano*, 4(10):6203-6211, 2010.

[87] Li, G. R., Wang, F., Jiang, Q. W., Gao, X. P., and Shen, P. W. Carbon nanotubes with titanium nitride as a low-cost counter electrode material for dye-sensitized solar cells. *Angewandte Chemie International Edition*, 49(21):3653-3656, 2010.

[88] Bönnemann, H., Khelashvili, G., Behrens, S., Hinsch, A., Skupien, K. and Dinjus, E. Role of the platinum nanoclusters in the iodide/triiodide redox system of dye solar cells. *Journal of Cluster Science*, 18(1):141-155, 2007.

[89] Fang, X., Ma, T., Guan, G., Akiyama, M. and Abe, E. Performances characteristics of dye-sensitized solar cells based on counter electrodes with Pt films of different thickness. *Journal of Photochemistry and Photobiology A: Chemistry*, 164(1-3):179-182, 2004.

[90] Fang, X., Ma, T., Guan, G., Akiyama, M., Kida, T., and Abe, E. Effect of the thickness of the Pt film coated on a counter electrode on the performance of a dye-sensitized solar cell. *Journal of Electroanalytical Chemistry*, 570(2):257-263, 2004.

[91] Papageorgiou, N., Maier, W. F., and Grätzel, M. An iodine/triiodide reduction electrocatalyst for aqueous and organic media. *Journal of The Electrochemical Society*, 144(3):876, 1997.

[92] Li, K., Yu, Z., Luo, Y., Li, D. and, Meng, Q. Recent progress of counter electrodes in nanocrystalline dye-sensitized solar cells. *Journal of Materials Science & Technology*, 23(5):577-+, 2007.

[93] Hauch, A. and Georg, A. Diffusion in the electrolyte and charge-transfer reaction at the platinum electrode in dye-sensitized solar cells. *Electrochimica Acta*, 46(22):3457-3466, 2001.

[94] Kakiage, K., Aoyama, Y., Yano, T., Oya, K., Fujisawa, J. I., and Hanaya, M. Highly-efficient dye-sensitized solar cells with collaborative sensitization by silyl-anchor and carboxy-anchor dyes. *Chemical Communications*, 51(88):15894-15897, 2015.

[95] Xu, Y., Bai, H., Lu, G., Li, C., and Shi, G. Flexible graphene films via the filtration of water-soluble noncovalent functionalized graphene sheets. *Journal of the American Chemical Society*, 130(18):5856-5857, 2008.

[96] Zhang, D. W., Li, X. D., Li, H. B., Chen, S., Sun, Z., Yin, X. J., and Huang, S. M.

Graphene-based counter electrode for dye-sensitized solar cells. *Carbon*, 49(15):5382-5388, 2011.

[97] Mathew, S., Yella, A., Gao, P., Humphry-Baker, R., Curchod, B. F., Ashari-Astani, N., Tavernelli, I., Rothlisberger, U., Nazeeruddin, M. K., and Grätzel, M. Dye-sensitized solar cells with 13% efficiency achieved through the molecular engineering of porphyrin sensitizers. *Nature Chemistry*, 6(3):242-247, 2014.

[98] Chiang, J. C. and MacDiarmid, A. G. "Polyaniline": Protonic acid doping of the emeraldine form to the metallic regime. *Synthetic Metals*, 13(1-3):193-205, 1986.

[99] Li, Q., Wu, J., Tang, Q., Lan, Z., Li, P., Lin, J., and Fan, L. Application of microporous polyaniline counter electrode for dye-sensitized solar cells. *Electrochemistry Communications*, 10(9):1299-1302, 2008.

[100] Park, K. H., Kim, S. J., Gomes, R., and Bhaumik, A. High performance dye-sensitized solar cell by using porous polyaniline nanotubes as counter electrode. *Chemical Engineering Journal*, 260:393-398, 2015.

[101] Chen, J., Li, B., Zheng, J., Zhao, J., Jing, H., and Zhu, Z. Polyaniline nanofiber/carbon film as flexible counter electrodes in platinum-free dye-sensitized solar cells. *Electrochimica Acta*, 56(12):4624-4630, 2011.

[102] Chiang, C. H., Chen, S. C., and Wu, C. G. Preparation of highly concentrated and stable conducting polymer solutions and their application in high-efficiency dye-sensitized solar cell. *Organic Electronics: physics, materials, applications*, 14(9):2369-2378, 2013.

[103] Gong, J., Liang, J., and Sumathy, K. Review on dye-sensitized solar cells (DSSCs): Fundamental concepts and novel materials. *Renewable and Sustainable Energy Reviews*, 16(8):5848-5860, 2012.

[104] Wu, J., Lan, Z., Lin, J., Huang, M., Huang, Y., Fan, L., and Luo, G. Electrolytes in dye-sensitized solar cells. *Chemical Reviews*, 115(5):2136-2173, 2015.

[105] Yu, Z., Vlachopoulos, N., Gorlov, M., and Kloo, L. Liquid electrolytes for dye-sensitized solar cells. *Dalton Transactions*, 40(40):10289-10303, 2011.

[106] Wu, J., Lan, Z., Lin, J., Huang, M., and Li, P. Effect of solvents in liquid electrolyte on the photovoltaic performance of dye-sensitized solar cells. *Journal of Power Sources*, 173(1):585-591, 2007.

[107] Boschloo, G. and Hagfeldt, A. Characteristics of the iodide/triiodide redox mediator in dye-sensitized solar cells. *Accounts of Chemical Research*, 42(11):1819-1826, 2009.

[108] Hara, K., Dan-oh, Y., Kasada, C., Ohga, Y., Shinpo, A., Suga, S., Sayama, K., and Arakawa, H. Effect of additives on the photovoltaic performance of coumarin-dye-sensitized nanocrystalline TiO_2 solar cells. *Langmuir*, 20(10):4205-4210, 2004.

[109] Boschloo, G., Häggman, L., and Hagfeldt, A. Quantification of the effect of 4-tert-

butylpyridine addition to I^-/I_3^- redox electrolytes in dye-sensitized nanostructured TiO_2 solar cells. *Journal of Physical Chemistry B*, 110(26):13144-13150, 2006.

[110] Hagfeldt, A. and Grätzel, M. Light-induced redox reactions in nanocrystalline systems. *Chemical Reviews*, 95(1):49-68, 1995.

[111] Rogers, R. D. and Seddon, K. R. Ionic liquids-solvents of the future? *Science*, 302(5646):792-793, 2003.

[112] Gorlov, M. and Kloo, L. Ionic liquid electrolytes for dye-sensitized solar cells. *Dalton Transactions*, 0(20):2655-2666, 2008.

[113] Li, F., Jennings, J. R., Wang, X., Fan, L., Koh, Z. Y., Yu, H., Yan, L., and Wang, Q. Influence of ionic liquid on recombination and regeneration kinetics in dye-sensitized solar cells. *Journal of Physical Chemistry C*, 118(30):17153-17159, 2014.

[114] Benedetti, J. E., Gonçalves, A. D., Formiga, A. L., De Paoli, M. A., Li, X., Durrant, J. R., and Nogueira, A. F. A polymer gel electrolyte composed of a poly(ethylene oxide) copolymer and the influence of its composition on the dynamics and performance of dye-sensitized solar cells. *Journal of Power Sources*, 195(4):1246-1255, 2010.

[115] Li, Q., Chen, H., Lin, L., Li, P., Qin, Y., Li, M., He, B., Chu, L., and Tang, Q. Quasi-solid-state dye-sensitized solar cell from polyaniline integrated poly(hexamethylene diisocyanate tripolymer/polyethylene glycol) gel electrolyte. *Journal of Materials Chemistry A*, 1(17):5326-5332, 2013.

[116] Li, Q., Wu, J., Tang, Z., Xiao, Y., Huang, M., and Lin, J. Application of poly(acrylic acid-g-gelatin)/polypyrrole gel electrolyte in flexible quasi-solid-state dye-sensitized solar cell. *Electrochimica Acta*, 55(8):2777-2781, 2010.

[117] Chen, C.-L., Teng, H., and Lee, Y.-L. Preparation of highly efficient gel-state dye-sensitized solar cells using polymer gel electrolytes based on poly(acrylonitrile-co-vinyl acetate). *Journal of Materials Chemistry*, 21(3):628-632, 2011.

[118] Yang, H., Huang, M., Wu, J., Lan, Z., Hao, S., and Lin, J. The polymer gel electrolyte based on poly(methyl methacrylate) and its application in quasi-solid-state dye-sensitized solar cells. *Materials Chemistry and Physics*, 110(1):38-42, 2008.

[119] Nogueira, A. F., Durrant, J. R., and De Paoli, M. A. Dye-sensitized nanocrystalline solar cells employing a polymer electrolyte. *Advanced Materials*, 13(11):826-830, 2001.

[120] Lee, H. C., Akhtar, M. S., Park, J. G., Kim, K. J., Lee, S. K., and Yang, O. Carbon nanotube (CNT)–polymethyl methacrylate (PMMA) composite electrolyte for solid-state dye sensitized solar cells. *Journal of Nanoscience and Nanotechnology*, 10(5):3502-3507, 2010.

[121] Tsai, C. H., Lu, C. Y., Chen, M. C., Huang, T. W., Wu, C. C., and Chung, Y. W. Efficient gel-state dye-sensitized solar cells adopting polymer gel electrolyte based on poly(methyl

methacrylate). *Organic Electronics: physics, materials, applications*, 14(11):3131-3137, 2013.

[122] Theerthagiri, J., Senthil, R. A., Buraidah, M. H., Madhavan, J., and Arof, A. K. Effect of tetrabutylammonium iodide content on PVDF-PMMA polymer blend electrolytes for dye-sensitized solar cells. *Ionics*, 21(10):2889-2896, 2015.

[123] Aram, E., Ehsani, M., and Khonakdar, H. A. Improvement of ionic conductivity and performance of quasi-solid-state dye sensitized solar cell using PEO/PMMA gel electrolyte. *Thermochimica Acta*, 615:61-67, 2015.

[124] Araujo, P. L. B., Araujo, E. S., Santos, R. F. S., and Pacheco, A. P. L. Synthesis and morphological characterization of PMMA/polyaniline nanofiber composites. *Microelectronics Journal*, 36(11):1055-1057, 2005.

[125] Shen, W., Deng, H., and Gao, Z. Synthesis of polyaniline via DNAzyme-catalyzed polymerization of aniline. *RSC Advances*, 4(95):53257-53264, 2014.

[126] Tang, Z., Wu, J., Liu, Q., Zheng, M., Tang, Q., Lan, Z., and Lin, J. Preparation of poly(acrylic acid)/gelatin/polyaniline gel-electrolyte and its application in quasi-solid-state dye-sensitized solar cells. *Journal of Power Sources*, 203:282-287, 2012.

[127] Sim, B. and Choi, H. J. Facile synthesis of polyaniline nanotubes and their enhanced stimuli-response under electric fields. *RSC Advances*, 5(16):11905-11912, 2015.

[128] Marchezi, P. E., Sonai, G. G., Hirata, M. K., Schiavon, M. A., and Nogueira, A. F. Understanding the role of reduced graphene oxide in the electrolyte of dye-sensitized solar cells. *Journal of Physical Chemistry C*, 120(41):23368-23376, 2016.

[129] Li, Q., Wu, J., Tang, Q., Lan, Z., Li, P., and Zhang, T. Application of polymer gel electrolyte with graphite powder in quasi-solid-state dye-sensitized solar cells. *Polymer Composites*, 30(11):1687-1692, 2009.

[130] Nath, B. C., Das, D., Kamrupi, I. R., Mohan, K. J., Ahmed, G. A., and Dolui, S. K. An efficient quasi solid state dye sensitized solar cell based on polyethylene glycol/graphene nanosheet gel electrolytes. *RSC Advances*, 5(115):95385-95393, 2015.

[131] Ou, R., Gupta, S., Parker, C. A., and Gerhardt, R. A. Fabrication and electrical conductivity of poly(methyl methacrylate) (PMMA)/carbon black (CB) composites: Comparison between an ordered carbon black nanowire-like segregated structure and a randomly dispersed carbon black nanostructure. *Journal of Physical Chemistry B*, 110(45):22365-22373, 2006.

[132] Lei, B. X., Fang, W. J., Hou, Y. F., Liao, J. Y., Kuang, D. B., and Su, C. Y. All-solid-state electrolytes consisting of ionic liquid and carbon black for efficient dye-sensitized solar cells. *Journal of Photochemistry and Photobiology A: Chemistry*, 216(1):8-14, 2010.

[133] Lee, C. P., Chen, P. Y., Vittal, R., and Ho, K. C. Iodine-free high efficient quasi solid-state

dye-sensitized solar cell containing ionic liquid and polyaniline-loaded carbon black. *Journal of Materials Chemistry*, 20(12):2356-2361, 2010.

[134] Yun, H. J., Jung, D. Y., Lee, D. K., Jen, A. K. Y., and Kim, J. H. Panchromatic quasi-solid-state squaraine dye sensitized solar cells enhanced by Förster resonance energy transfer of DCM-pyran. *Dyes and Pigments*, 113:675-681, 2015.

[135] Yao, N., Huang, J., Fu, K., Deng, X., Ding, M., and Xu, X. Rare earth ion doped phosphors for dye-sensitized solar cells applications. *RSC Advances*, 6(21):17546-17559, 2016.

[136] Wang, Y. and Hu, A. Carbon quantum dots: Synthesis, properties and applications. *Journal of Materials Chemistry C*, 2(34):6921-6939, 2014.

[137] Fernando, K. S., Sahu, S., Liu, Y., Lewis, W. K., Guliants, E. A., Jafariyan, A., Wang, P., Bunker, C. E., and Sun, Y. P. Carbon quantum dots and applications in photocatalytic energy conversion. *ACS Applied Materials and Interfaces*, 7(16):8363-8376, 2015.

[138] Lim, S. Y., Shen, W., and Gao, Z. Carbon quantum dots and their applications. *Chemical Society Reviews*, 44(1):362-381, 2015.

[139] Wang, H., Sun, C., Chen, X., Zhang, Y., Colvin, V. L., Rice, Q., Seo, J., Feng, S., Wang, S., and William, W. Y. Excitation wavelength independent visible color emission of carbon dots. *Nanoscale*, 9(5):1909-1915, 2017.

[140] Khan, W. U., Wang, D., Zhang, W., Tang, Z., Ma, X., Ding, X., Du, S., and Wang, Y. High quantum yield green-emitting carbon dots for Fe(III) detection, biocompatible fluorescent ink and cellular imaging. *Scientific Reports*, 7(1):14866, 2017.

[141] Zhu, S., Meng, Q., Wang, L., Zhang, J., Song, Y., Jin, H., Zhang, K., Sun, H., Wang, H., and Yang, B. Highly photoluminescent carbon dots for multicolor patterning, sensors, and bioimaging. *Angewandte Chemie International Edition*, 52(14):3953-3957, 2013.

[142] Diantoro, M., Suprayogi, T., Hidayat, A., Taufiq, A., Fuad, A., and Suryana, R. Shockley's equation fit analyses for solar cell parameters from I-V curves. *International Journal of Photoenergy*, 2018:1-7, 2018.

[143] Koide, N., Islam, A., Chiba, Y., and Han, L. Improvement of efficiency of dye-sensitized solar cells based on analysis of equivalent circuit. *Journal of Photochemistry and Photobiology A: Chemistry*, 182(3):296-305, 2006.

[144] Snaith, H. J., Schmidt-Mende, L., Grätzel, M., and Chiesa, M. Light intensity, temperature, and thickness dependence of the open-circuit voltage in solid-state dye-sensitized solar cells. *Physical Review B:Condensed Matter and Materials Physics*, 74(4):045306, 2006.